

Mesoscopic architecture enhances communication across the macaque connectome revealing structure-function correspondence in the brain

Anand Pathak ^{1,2}, Shakti N. Menon ¹ and Sitabhra Sinha ^{1,2}

¹The Institute of Mathematical Sciences, CIT Campus, Taramani, Chennai 600113, India

²Homi Bhabha National Institute, Anushaktinagar, Mumbai 400 094, India

 (Received 9 July 2021; revised 6 June 2022; accepted 13 September 2022; published 9 November 2022)

Analyzing the brain in terms of organizational structures at intermediate scales provides an approach to unravel the complexity arising from interactions between its large number of components. Focusing on a wiring diagram that spans the cortex, basal ganglia, and thalamus of the macaque brain, we identify robust modules in the network that provide a mesoscopic-level description of its topological architecture. Surprisingly, we find that the modular architecture facilitates rapid communication across the network, instead of localizing activity as is typically expected in networks having community organization. By considering processes of diffusive spreading and coordination, we demonstrate that the specific pattern of inter- and intramodular connectivity in the network allows propagation to be even faster than equivalent randomized networks with or without modular structure. This pattern of connectivity is seen at different scales and is conserved across principal cortical divisions, as well as subcortical structures. Furthermore, we find that the physical proximity between areas is insufficient to explain the modular organization, as similar mesoscopic structures can be obtained even after factoring out the effect of distance constraints on the connectivity. By supplementing the topological information about the macaque connectome with physical locations, volumes, and functions of the constituent areas and analyzing this augmented dataset, we reveal a counterintuitive role played by the modular architecture of the brain in promoting global coordination of its activity. It suggests a possible explanation for the ubiquity of modularity in brain networks.

DOI: [10.1103/PhysRevE.106.054304](https://doi.org/10.1103/PhysRevE.106.054304)

I. INTRODUCTION

Cortical functional localization, which refers to specific areas of the cerebral cortex being associated with distinct functions such as vision and language, has long been a dominant paradigm in neuroscience [1]. As the connectome provides a physical substrate for cognition and behavior [2,3], it might seem intuitive that such localization could be reflected in the structural attributes of the network [4]. However, brain imaging studies show that a large number of areas become active during any cognitive task, ruling out the possibility of attributing specific functions to the activation of a particular subset of vertices of the structural connectome [5]. This suggests the necessity for a theoretic framework that investigates the dynamics of the brain in terms of how different areas connect and interact with each other [6]. Such an approach should integrate complementary perspectives that focus on (a) dynamics, where *distributed* activation of the entire network converges to different attractors, and (b) computation, in which *localized* processing of information occurs in a sequential manner, allowing us to interpret cognitive processing as dynamical computation [7].

An integrated view of how local and global coordination of activity across the brain can arise may be obtained by adopting a mesoscopic approach to analyzing the connectome. Such an approach focuses on understanding the interactions within and between communities of densely interconnected brain areas

(*modules*) that have been identified in nervous systems of different organisms [8–18]. Such structural modularity of the brain is expected from the advantages that such an architecture may confer during evolution and development [16,19], such as imparting robustness in the presence of constraints on wiring and performance [3,20,21]. Traditionally, modules have been viewed in functional terms, associated with innate, domain-specific mental faculties (such as language) that are believed to be relatively independent of each other [22]. Examining how such cognitive modules relate to the structural communities of the connectome addresses the fundamental issue of structure-function correspondence in the brain [23,24].

In this paper, we focus on the structure-function relation revealed by the modular structure of the macaque connectome. We suggest that this mesoscopic organizational feature balances specialized and integrated processing by allowing rapid communication at both local and global scales. This is striking in view of the role that modularity plays in promoting information encapsulation in other network architectures [25]. In contrast, we observe that the specific pattern of intra- and intermodular connectivity among the macaque brain areas enables extremely rapid communication, not only locally within each module, but surprisingly, also globally across the entire network. Indeed, we show using general models of diffusion as well as coordination dynamics that spreading occurs significantly faster in the empirical network, not only compared to modular surrogate networks but also with respect

to homogeneous randomized networks. As one associates the latter class of networks with maximal propagation rate, which is expected to reduce when community organization is introduced, our results may appear counterintuitive. A detailed investigation of the structural organization suggests that these features could be related to the preferential connections between certain classes of brain areas that serve specific roles in connecting members of a community and/or those belonging to different communities. This result has potential implications not only for other brain networks, but generally for modular networks that are involved in information processing, complementing studies showing that maximizing information flow may cause model networks to evolve towards a modular structure [26,27].

In performing our analysis, we have added curated spatial and functional information concerning the brain areas to the existing database of brain connectivity, which can serve as a resource for the community. The modules revealed by our analysis, which we have shown to be robust across many possible partitionings of the network using different techniques, builds upon earlier work [9,13,18] by including subcortical regions of the connectome. We show that each module comprises both cortical and subcortical components, which is intriguing in view of the proposal that the thalamocortical loop plays a central role in the computational architecture of the neocortex [28]. More crucially, while it has been suggested earlier that physical space constraints cannot exclusively account for modules [11,29,30], our determination of the space-independent modules and their relatively high overlap with the original communities clearly indicate that the modularity of the macaque brain has functional significance, viz., the facilitation of communication across the connectome.

II. MATERIALS AND METHODS

A. Data

1. Connectivity

We have used as the basis for reconstructing the macaque connectome a directed network of brain areas (cortical and subcortical) that was compiled in Ref. [31] using several hundred tract tracing studies obtained from CoCoMac—a comprehensive neuroinformatics database [32–34]. The original network comprised 383 vertices (or nodes), representing areas in the cortex, basal ganglia and thalamus, at different levels of spatial resolution, and 6602 directed edges (or links) corresponding to tracts, i.e., myelinated bundles of axons connecting different brain areas, which may span large distances. We note that while there have been later studies reporting additional connections between specific brain areas (e.g., Ref. [35]), these are likely to only incrementally augment the substantial number of links already incorporated in the network. The different regions and areas of the brain are represented in the network in a hierarchically organized arrangement, starting from the most coarse-grained level corresponding to the entire brain. As a result, the same subdivision may occur multiple times in the network, as a vertex could represent an area that is part of a larger area or region which is represented by a different vertex (see

Supplemental Material, Fig. S1 [36]). For example, the hippocampus is a vertex of the network, as are its subdivisions CA1, CA3, and Dentate Gyrus. Consequently, there is no unique mapping between brain areas and the vertices of this network. It also leads to ambiguity in interpreting edges connecting vertices that occur at any of the levels other than the lowest one in the hierarchy. For instance, if both vertices A and B link to C, but B is a subdivision of A, then it is unclear if the two edges are distinct. These issues make it difficult to interpret any results obtained by analyzing the original network [36].

In the connectome we consider here, these issues are avoided by considering only those vertices that occur at the lowest hierarchical level, i.e., corresponding to areas with no further subdivisions, in the original network. This yields an unweighted network comprising 266 vertices, representing brain areas that span a range of spatial scales ranging from the visual cortex area V1 (which has a volume of $\sim 2000 \text{ mm}^3$) to the thalamic area PT#2 (which has a volume of less than 2 mm^3). The network that we consider, consequently, consists of the 2602 directed links that occur between these vertices. Note that this procedure leads to the network having a largest connected component of 261 vertices (as the following five areas do not have any reported connections to the other areas at the lowest hierarchical level: PT#2, 6b-beta, 4a, 4b, and Sub.Th). Despite the reduction in the size of the network upon removal of the aforementioned redundancies, the resulting connectome has similar macroscopic properties as the original network, such as the exponential nature of the degree distribution (see Supplemental Material, Fig. S2 [36]).

As tracts can be of varying widths, in principle, it is possible to consider a weighted network of brain areas, the weight associated with each link being proportional to the thickness of the tract connecting the two regions. However, it is not known whether any simple relation exists between tract thickness and the interaction strength between the regions it connects, and hence it is unclear how to interpret the results of any mesolevel analysis that takes into account thickness information [37]. We note that the original network of brain areas [31] was reconstructed using data from more than 400 separate studies spanning several decades. The various connections reported in these studies do not use a consistent format, neither can standardization of, e.g., injection sites be expected. Indeed, even the terminology used to refer to the areas differ between the studies. Thus, these needed to be mapped to a single framework in Ref. [31] using a particular atlas before the network representing the connectome could be reconstructed from the data.

2. Spatial positions

As the brain connectome is a spatially embedded network, it is important to consider geometric information such as physical locations and extent of the different brain areas, in addition to the connection topology. As the original network [31] did not contain any spatial information, we have compiled a comprehensive database of the positions of the areas corresponding to each of the vertices, as well as, the volumes spanned by them. We have obtained the

stereotaxic coordinates of each brain area in our connectome from several sources. Information about 134 of the 266 areas included in the connectome has been obtained from the website associated with the Paxinos Rhesus Monkey Atlas [38]. For the remaining areas, we manually curated the requisite data from the relevant research literature. The position of an area is identified with the approximate location of its center obtained from the online three-dimensional visualization platform in the website mentioned above [38]. The volume spanned by a particular area was estimated by approximating its cross-section extent in each of the coronal sections of the brain and obtaining their sum, weighted by the thickness of the sections measured along the rostral-caudal axis. See `connectome_nodes.xls` [36] for the three-dimensional coordinates of, and the volumes covered by, each of the brain areas that we obtained through the above analysis. It also lists the references that were used to obtain the information in each case.

3. Data Availability

The adjacency list `connectome_links.xls` [36] contains information about the directed connections between the brain areas, with the first column indicating the source vertex and the second column the target vertex (both vertices being represented by their serial number as given in `connectome_nodes.xls`). The table `connectome_nodes.xls` [36] is a spreadsheet comprising 11 columns which contain information about each of the 266 brain areas which correspond to the vertices of the network. The first 7 columns provide the identity of each area in terms of the serial number by which they are identified in our study, the abbreviation, the name, their position in the macaque brain described in terms of the three-dimensional coordinates as per the Paxinos atlas and the volume that they occupy. The eighth and ninth columns contain information arising from our analysis, viz., the module they belong to and their role in the mesoscopic organization, respectively. The last two columns contain, respectively, the references and the web resources from which we have gleaned information about their positions and volumes.

B. Modularity

A prominent mesoscopic structural property associated with many networks that occur in nature is modular organization. Modules (or communities) are subnetworks that are characterized by a higher density of connections between the constituent nodes compared to that between nodes belonging to different modules [39]. One of the most well-known approaches for determining the modules of a network is to maximize a quantitative measure, Q , defined for a given modular partitioning of the network as, $Q = L^{-1} \sum_{i,j} B_{ij} \delta_{c_i c_j}$, where $B_{ij} = A_{ij} - (k_i^{\text{in}} k_j^{\text{out}} / L)$ are elements of the modularity matrix \mathbf{B} [40,41]. The adjacency matrix \mathbf{A} ($A_{ij} = 1$, if a directed link exists from j to i , and 0, otherwise) specifies the connection topology of the network, while the number of incoming and outgoing connections of node i are indicated by the in-degree $k_i^{\text{in}} = \sum_j A_{ij}$ and out-degree $k_i^{\text{out}} = \sum_j A_{ji}$, respectively, with $L (= \sum_j k_j^{\text{in}} = \sum_j k_j^{\text{out}})$ being the total number of connections in the network. The Kronecker δ function δ_{ij}

yields 1 if the communities c_i and c_j to which nodes i and j belong respectively, are identical, and is 0 otherwise.

1. Spectral analysis and its refinement

To achieve an optimal partitioning of the network through the maximization of Q we have used the spectral method [41]. Here, we first bisect the network by assigning nodes to one of two communities according to the sign of the elements of the eigenvector corresponding to the largest positive eigenvalue of the symmetrized modularity matrix $\mathbf{B} + \mathbf{B}^T$. Subsequently we refine the partition by swapping the nodes between communities to achieve the highest possible value of Q . The above procedure is carried out recursively on each of the communities to further subdivide them until Q cannot be increased further [41]. This approach yields a maximum value of Q for a partitioning of the network into 5 modules with $Q_{\text{spectral}} = 0.485$.

2. Multiscale analysis of community organization

Techniques that detect communities in networks by maximizing Q typically have a resolution limit which places a lower bound on the size of modules that can be identified [42]. To circumvent this limit and detect modules that span the entire range of possible sizes, the definition of Q has been augmented by the inclusion of a resolution parameter γ [29,43,44] in the definition of the modularity matrix \mathbf{B} , viz., $B_{ij} = A_{ij} - \gamma(k_i^{\text{in}} k_j^{\text{out}} / L)$. Note that the standard definition of Q corresponds to $\gamma = 1$. By increasing γ , modules obtained at a coarser level of resolution can, in principle, be fragmented further, thereby yielding smaller modules. To obtain the modular partitions of the network at different levels of resolution, we have applied the spectral method on the suitably modified modularity matrix \mathbf{B} .

3. Robustness of the partitioning

To ensure that the modular partitions of the network obtained using the deterministic spectral technique (described above) are not sensitively dependent on the specific method used for maximizing Q , we have used the stochastic simulated annealing approach to obtain an ensemble of 10^3 optimal partitions. The dissimilarity between the different partitions generated by each realization of the annealing technique reflects the extent of degeneracy (and hence, ambiguity) inherent in the modular decomposition of the network. Following Ref. [45], for each realization of the simulated annealing approach we begin with an arbitrary partition of the network and iteratively change the modular composition by implementing one of three types of operations: (i) move a randomly chosen node to any other module including a newly created one, (ii) merge two randomly chosen modules, and (iii) split a randomly chosen module into two parts to minimize the number of connections between the two parts. Any one of the possible operations (across all types) is chosen at each step with equal probability. The resulting partition associated with a change ΔQ in the modularity is accepted with a probability $\exp(-|\Delta Q|/T)$ if $\Delta Q < 0$ and $p = 1$ otherwise. Here, the parameter T , which is analogous to temperature, is decreased over time according to a specified cooling schedule. The process terminates when the number of successive failures at

altering the modules exceeds a threshold value. While the Q values corresponding to the partitions obtained for different realizations span a wide range, most of them cluster around that obtained from the spectral method, Q_{spectral} . We focus on the 291 partitions whose Q value deviates from Q_{spectral} by less than 3%. As shown later, the modular membership of 70% of the nodes remain invariant across all of these partitions, and are in fact identical to that obtained from the spectral method, underlining the robustness of the modular decomposition. We have also used alternative methods of module identification that do not rely on maximizing Q , viz., the Infomap method [46], and have obtained qualitatively similar results.

4. Consensus clustering and versatility

To quantify the consistency among the various modular partitionings obtained using simulated annealing method, we define a consensus matrix \mathbf{P} as described in Ref. [47]. The consensus matrix is defined such that P_{ij} indicates the fraction of partitionings in which nodes i and j appear in the same module out of total number of partitionings obtained from the simulated annealing realizations. Note that $P_{ij} = 0$ and 1 corresponds, respectively, to situations where the nodes i and j always appear in the same module for every partitioning, and where they never occur in the same module.

A measure for the certainty with which a brain area is assigned to a module of the network is provided by the versatility metric described in [48]. Using the consensus matrix \mathbf{P} for the network, the versatility of node i is calculated as $V_i = \sum_j \sin(\pi P_{ij}) / \sum_j P_{ij}$. Versatility of i is highest when $P_{ij} = 0.5$ for all $j \neq i$, while it is lowest when P_{ij} is either 0 or 1 for any j . In the latter case, the other nodes belonging to the module in which node i occurs in any given partitioning are always the same. Thus, a low value of versatility indicates stable modular membership of the node.

C. Classification of brain areas according to their role in the mesoscopic structural organization of the connectome

The importance of a given area within the topological organization of the macaque brain network is indicated by its connectivity within its own module (as defined above), as well as that across the entire brain, which is evident from its connections to areas belonging to other modules. These can be quantitatively measured by the metrics (i) the within module degree z score (z) and (ii) the participation coefficient (Π^c), respectively [49,50]. To identify areas that have significantly more connections within their own module, we determine a within module degree z score:

$$z_i = \frac{k_{c_i}^i - \langle k_{c_i}^j \rangle_{j \in c_i}}{\sqrt{(\langle k_{c_i}^j \rangle_{j \in c_i})^2 - \langle k_{c_i}^j \rangle_{j \in c_i}^2}}, \quad (1)$$

where $k_{c_i}^i$ is the number of links between area i and other areas belonging to its module (c_i) and the average $\langle \dots \rangle_{j \in c_i}$ is taken over all areas in a module c . As in Refs. [11,51], nodes (areas) having $z > 0.7$ are identified as hubs, the remainder being classified as nonhubs.

To distinguish between brain areas in terms of their inter-modular connectivity we calculate the participation coefficient Π_i^c of area i as

$$\Pi_i^c = 1 - \sum_{c=1}^m \left(\frac{k_c^i}{k^i} \right)^2, \quad (2)$$

where k_c^i is number of links that area i has with those areas belonging to module c and $k^i = \sum_c k_c^i$ is the total degree of the i th node (area). An area whose connections are restricted within its own module has $\Pi_i^c = 0$ while one whose links are uniformly distributed among the different modules has Π_i^c closer to 1. Based upon the value of Π_i^c , which provides a measure of how well a node (area) bridges different modules, the nonhub areas are classified as ultraperipheral (R1, $\Pi^c \leq 0.05$), peripheral (R2, $0.05 < \Pi^c \leq 0.62$), satellite connectors (R3, $0.62 < \Pi^c \leq 0.8$), and kinless nodes (R4, $\Pi^c > 0.8$), while the hubs can be demarcated into provincial hubs (R5, $\Pi^c \leq 0.3$), connector hubs (R6, $0.3 < \Pi^c \leq 0.75$), and global hubs (R7, $\Pi^c > 0.75$).

D. Degree- and modularity-preserved network randomization

We construct an ensemble of 10^3 networks obtained by randomizing the empirical network preserving the in-degree and out-degree of each node (area) as well as the modular organization of the network [11]. Each network is obtained by selecting directed connections, e.g., $i \rightarrow p$ and $j \rightarrow q$, such that the source nodes i, j belong to the same module A and target nodes p, q belong to the same module B (which could be same as A), and then rewire them to have $i \rightarrow q$ and $j \rightarrow p$. This procedure is repeated for 10^6 times for each realization of a randomized network. To randomize the network preserving the degree alone, we follow the same procedure as above with the difference that there is no constraint on the modular membership of the nodes.

E. Diffusive spreading model

The function of the connectome is to facilitate communication between the different brain areas. While the exact mechanism by which such communication occurs may be quite complex and not yet fully understood, different studies suggest that the anatomical network is a critical (although perhaps, not the only) determinant of this process [52–54]. We consider the simple process of diffusion across the system to investigate the role of the empirically observed pattern of intra- and intermodular connections on the dissemination of information in the brain network. For this purpose, we consider discrete random walks that, starting from a given node on the network, proceeds at each time step from one node to a randomly chosen node that receives an outwardly directed link from the former. The rate at which spreading occurs in different parts of the system can be analyzed by obtaining the distribution of first passage times (FPTs) for a random walk to reach a target node starting from a source node. For this, we have measured the FPTs τ to all nodes that are visited by a walk initiated from a given node of the network. The process is repeated 10^3 times starting from each of the 266 nodes, with a walk terminating when either every node has been visited at least once or a node with no

outgoing connections is reached. Separate distributions for intramodular FPTs (τ^{intra}) and intermodular FPTs (τ^{inter}) can be obtained by considering the source and target nodes to be in the same module or in different modules, respectively. For comparison, we also compute the distributions of FPTs τ_D and τ_{DM} for randomized surrogates in which either the degrees, or both the degrees and modular memberships, of the nodes are preserved, respectively. The distributions are obtained by averaging over 20 different networks, where in each case 10^3 stochastic realizations are performed starting from each of the 266 nodes of the network in turn. The deviation of the empirical FPT distribution from those obtained from the randomized surrogates by averaging over multiple realizations is quantified in terms of a z score measure defined as

$$z = \frac{P_{\text{emp}}(\tau) - \langle P_{\text{rand}}(\tau) \rangle}{\sqrt{\langle P_{\text{rand}}(\tau)^2 \rangle - \langle P_{\text{rand}}(\tau) \rangle^2}}, \quad (3)$$

where $P_{\text{emp}}(\tau)$ and $P_{\text{rand}}(\tau)$ are the empirical and randomized surrogate FPT distributions, respectively.

F. Model for collective ordering

To ensure that our results about the ability of the empirical network to allow rapid communication is not sensitively dependent on the diffusive spreading model used, we have also investigated the onset of collective ordering in such networks using a modeling framework inspired by statistical physics [21,55,56]. In particular, we use the Ising model paradigm, wherein classical binary-state spins dynamically change their orientation based on thermal fluctuations (corresponding to noise that represents deviations from deterministic dynamics arising from stochastic effects, delays, external signals, etc. [57]) and interactions with neighboring spins (that correspond to coupling mediated by the network connecting the different nodes). Each spin σ_i can be in any one of two possible orientations, viz., UP (+1) or DOWN (−1), which can be interpreted as the mean activity of a brain region i being either high or low, respectively [58]. In this approach, a global function of the collective dynamical state of the system comprising N spins is defined, usually in terms of a Hamiltonian $\mathcal{H}(\sigma)$ where $\sigma = \{\sigma_1, \sigma_2, \dots, \sigma_N\}$, such that the dynamical evolution of the system proceeds by minimization of the function. Thus, if switching the orientation of a spin i from σ_i to $-\sigma_i$ results in a change in this function by an amount $\Delta\mathcal{H}(\sigma_i \rightarrow -\sigma_i) = \sigma_i \sum_j A_{ij} \sigma_j$, where A_{ij} is an element of the directed adjacency matrix ($= 1$ if there is a connection from node j to i , and $= 0$, otherwise), then the move is accepted with a probability $P = \min(e^{-\frac{\Delta\mathcal{H}}{T}}, 1)$. The temperature T (scaled by the Boltzmann constant k_B) quantifies the noise present in the system. We evolve the system at a given temperature T from an initially random configuration of σ using a Monte Carlo (MC) algorithm [59], at each step sequentially choosing N spins at random and attempting to update their orientation following the procedure mentioned above. For each realization, we continue the procedure until the system reaches an equilibrium configuration of σ characterized by the long-time average of the order parameter $m = \sum_i \sigma_i / N$ attaining a steady state value m_∞ . To reduce the fluctuations in the time-series of m , it is smoothed by averaging over a moving window

of length 50 MC steps (we have verified that our results do not alter qualitatively upon using different window sizes). Convergence time t^{conv} is defined as the number of MC steps required by the system for the order parameter to reach m_∞ for the first time. The convergence behavior seen for the empirical network (averaged over 10^4 random initial conditions) have been compared with those observed in 25 different realizations each of degree-preserved (RD) and degree-preserved module-preserved (RDM) randomized networks. For each of the randomized networks, results are averaged over 10^3 random initial conditions.

G. Role of spatial geometry in the modular organization of the connectome

The physical distance d_{ij} between two brain areas i and j , whose centers are indicated by the vectors \mathbf{x} and \mathbf{y} , respectively, has been measured in terms of the Euclidean metric $d(\mathbf{x}, \mathbf{y})$ and scaled by the geometric mean of the radii r_i, r_j of the two areas (the radius of each being estimated from its volume).

1. Space-independent partitioning of the network into communities

For networks whose nodes are embedded in a space associated with a metric, it can be argued that the network properties, such as modularity, could be a consequence of the constraints imposed by the underlying geometry. We therefore need to modify the method for determining the modular structure of a network outlined above, to take into account the role of the physical space in which the network is embedded. This is done by redefining the modularity matrix \mathbf{B} in the definition of the quantity Q (given above), so that the expectation of a pair of nodes (i, j , say) being connected by chance in the null model incorporates the physical distance (d_{ij}) between the nodes. Thus, following Ref. [60], we redefine $B_{ij} = A_{ij} - (k_i^{\text{in}} k_j^{\text{out}} f(d_{ij}) / L)$, where $f(d) = \sum_{d_{ij}=d} A_{ij} / (k_i^{\text{in}} k_j^{\text{out}})$ is referred to as the *deterrence function*. This function, which is estimated from empirical data for the network, contains information about how the physical distance between a pair of nodes modulates their connection probability. Note that if the communities in the network arise entirely because of spatial dependence, measuring Q taking into account the physical distance between nodes does not yield any modular structure. Moreover, comparing the space-independent modular decomposition of the network obtained using this technique with the communities determined using exclusively information about the connection topology (as described earlier), we can infer whether the observed modularity is primarily driven by physical distance constraints. The similarity between the communities obtained using the two methods is quantified using *normalized mutual information*.

2. Normalized mutual information

To quantify the similarity between two modular decompositions $\{c_i^A\}_{i=1}^{M_A}$ and $\{c_j^B\}_{j=1}^{M_B}$ resulting from different partitionings A and B of a network (that yield M_A and M_B modules, respectively) we have used the normalized mutual

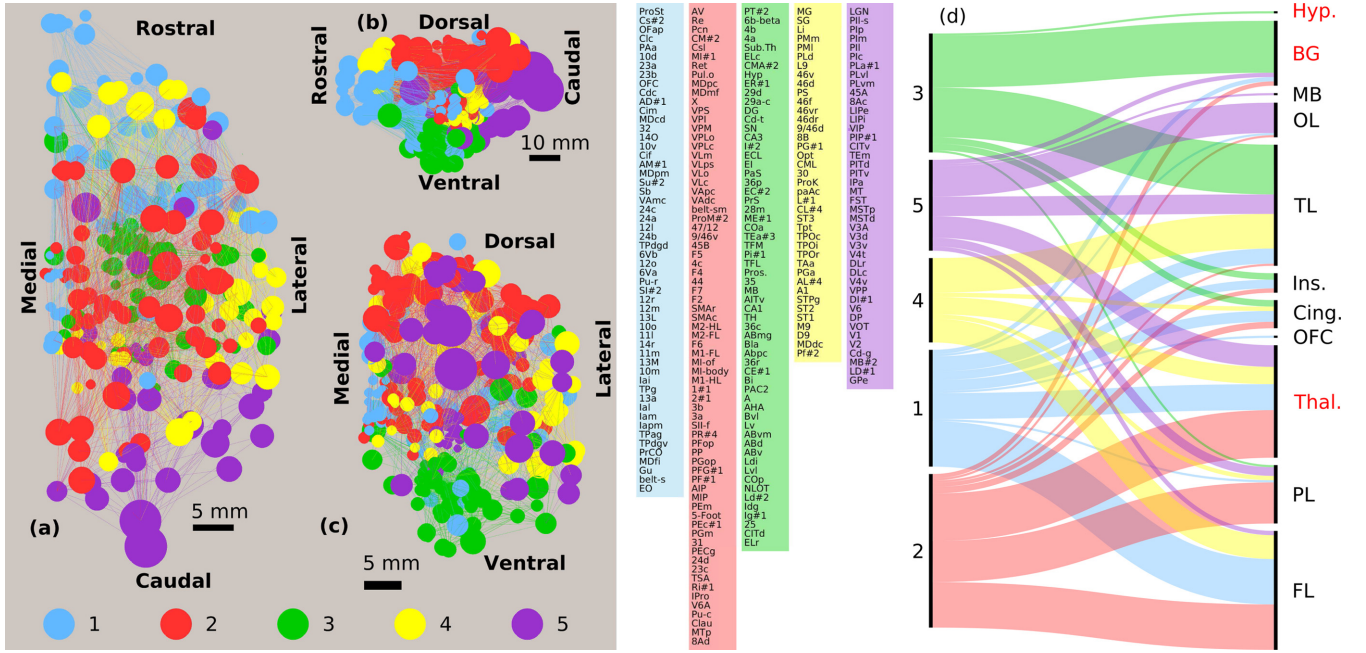


FIG. 1. Mesoscopic organization of the macaque brain. The network of brain areas, shown in (a) horizontal, (b) sagittal, and (c) coronal projections, clearly indicate that the nodes (filled circles) are organized into five modules, each characterized by dense intraconnectivity. The modular membership of each node is represented by its color (see color key to the right, containing the list of brain areas in each module), while node sizes provide a representation of the relative volumes of the corresponding brain areas (the spatial scale being indicated by the horizontal bar in each panel). The spatial positions of the nodes are specified by the three-dimensional stereotaxic coordinates of the corresponding areas (see Sec. II). Links indicate the directed nerve tracts connecting pairs of brain areas, and are colored in accordance with their source nodes. For details of each of the brain areas see `connectome_nodes.x1s` [36], and for the macroscopic properties of the network see Supplemental Material, Fig. S2 [36]. (d) Visual representation of the association between the network modules and cortical (in black), as well as, subcortical (in red) divisions of the brain, viz., *FL*: Frontal Lobe, *PL*: Parietal Lobe, *TL*: Temporal Lobe, *OL*: Occipital Lobe, *Cing.*: Cingulate gyrus, *Ins.*: Insula, *BG*: Basal Ganglia, *Thal.*: Thalamus, *Hyp.*: Hypothalamus, *OFC*: Olfactory complex, and *MB*: Mid-brain. For a detailed breakdown of the major subdivisions of the brain in terms of their module membership, see Supplemental Material, Table S1, as well as, Figs. S3 and S4 [36]. All alluvial diagrams in this paper have been created using the online visualization tool RAW [62].

information [61]

$$I_{\text{norm}}(A, B) = \frac{2 \sum_i \sum_j P(c_i^A, c_j^B) \ln [P(c_i^A, c_j^B) / P(c_i^A)P(c_j^B)]}{-\sum_i P(c_i^A) \ln P(c_i^A) - \sum_j P(c_j^B) \ln P(c_j^B)}, \quad (4)$$

where $P(c_i^A)$ is the probability that a randomly chosen node lies in module c_i^A in partition A , $P(c_j^B)$ is the probability that a randomly chosen node lies in module c_j^B in partition B , and $P(c_i^A, c_j^B)$ is the joint probability that a randomly chosen node belongs to module c_i^A in partition A , as well as, to module c_j^B in partition B ($i = 1, \dots, M_A$, and $j = 1, \dots, M_B$). Each of the probabilities can be estimated from the ratio of the community sizes to the size of the entire network.

3. Surrogate networks

To explicitly show that the modular organization is not primarily driven by the constraints imposed by the physical distance d between brain areas, we have demonstrated how spatial embedding affects the modular decomposition of a network, using three classes of surrogate random network ensembles (of size 100 each) having different underlying spatial dependencies. The three ensembles, in increasing order of importance of d in governing the connection probabil-

ity P between nodes, comprise networks with (a) $P \sim d^0$, (b) $P \sim d^{-1}$, which is the case in the empirical network, and (c) $P \sim \exp(-d)$, with nodes in each network occupying the same spatial position as in the empirical network. Each network (comprising an identical number of nodes and links as in the empirical network) was subject to community detection using information about the connection topology alone, as well as, space-independent modular decomposition, following the two approaches described above. The difference between these two sets of partitions provides a measure of the role that spatial embeddedness of the networks plays in determining the modular nature of their connectivity.

III. RESULTS

A. Mesoscopic organization of brain areas in the macaque

Figures 1(a)–1(c) show the modular organization of the macaque brain network spanning areas from the cortex, basal ganglia and thalamus, revealed by our analysis (for details see methods). The network is seen to comprise five modules, each module i being composed of m_i densely interconnected brain areas (their numbers ranging between 39 and 71, see the color key to the right of Figs. 1(a)–1(c), containing the list of brain areas in each module). The membership of

the individual areas in these modules is seen to be robust (as discussed in detail in the next subsection). Given that the network is embedded in a specific geometry, namely that of the macaque brain, it is noteworthy that each of the modules are spatially clustered as is clearly seen from the projections shown in Figs. 1(a)–1(c). To understand the implications of the spatial location of these modules, we visually represent the mapping between the modules and the major anatomical divisions of the brain in Fig. 1(d). For a detailed breakdown of the major divisions of the brain in terms of their module membership, see Supplemental Material, Table S1, as well as, Figs. S3 and S4 [36].

We observe that every module comprises sizable number of both cortical and subcortical areas. With the exception of module 3, the modules have their subcortical components located almost exclusively in the *Thalamus*. We note that each of these modules are associated with different sensory modalities (discussed in detail later), consistent with one of the primary functions of the *Thalamus*, namely, relaying information from the sensory organs to cortical areas for further processing. As the *Thalamus* is also involved in sleep-wake regulation coordinated via extensive reciprocal connections with the cortex [63–65], it is reasonable to expect that the each of the network modules will have thalamic components along with cortical ones, with dense intramodular connectivity representing thalamo-cortico-thalamic circuits [66,67]. However, none of the subcortical components of module 3 (displayed in green in Fig. 1) belong to the *Thalamus* and instead constitutes almost the entirety of the *Basal Ganglia*.

The locations of the cortical components of the different modules across the principal lobes of the cortex, viz., *frontal*, *temporal*, *parietal*, and *occipital*, are indicated in Fig. 1(d). We observe that there is no simple correspondence between the modules, which are topological partitions of the connectome, and the gross anatomical divisions of the cortex. While the regions comprising the frontal and temporal lobes are split between several modules, those in the parietal and occipital are dominated by single modules (modules 2 and 5, respectively), indicating the relative homogeneity of the latter lobes in the mesoscopic organization of the network. This is particularly important in light of a possible connection between the modular divisions and functional specialization in the brain—a point that we discuss below.

As mentioned in the Introduction, the term *module* has been primarily used in the neuroscience literature to refer to a functionally integrated set of areas [68–70] that allows for “information encapsulation” [22], whereas we employ the term in the sense of a specific mesolevel structural feature in the connectome [8–16]. In analogy with other biological networks where a structure-function correlation has been established for modules [49,71], we now ask whether the network modules that appear as separate structural units of the brain can be considered as distinct functional units as well. Using information about the known functions of different cortical and subcortical areas obtained from decades of experimental studies, we have created a mapping between the areas belonging to each module and the specific functionalities attributed to them. In Supplemental Material, Table S2 [36] we list these known functions either of the brain areas belonging to each of the modules, or of the broader subdivisions to which they belong.

A perusal of this information reveals that the different areas belonging to a module complement each other in carrying out various cognitive functions. For example, several cortical areas in module 5, viz., 45a and 8Ac of the prefrontal cortex, and V1 and V2 of the occipital lobe, are related through their involvement in vision, even though they may be part of distinct lobes and have disparate functions (controlling saccadic eye movements in the case of 45a and 8Ac, and processing of visual information in the case of V1 and V2). This suggests a general scheme of organization in which the areas associated with each of the principal sensory modalities are localized in specific modules, viz., visual in module 5, auditory in module 4, somatosensory (along with the principal motor area M1) in module 2, and olfactory (as well as, gustatory) in module 1. We show below that the known behavior of the areas comprising each of the modules is consistent with the broad functions attributed to that module.

First, we observe that module 5 (displayed in purple in Fig. 1) consists of the primary visual area in the occipital lobe and association areas in the parietal (e.g., LIP, VIP, etc.) and temporal lobe (e.g., CIT, PIT, etc.). In addition, its thalamic component includes lateral geniculate nucleus (LGN), which relays visual information to the cortex from the retina. We note that these areas are all involved in various aspects of visual cognition, which is consistent with the sensory modality associated with this module, viz., vision. Second, module 4 (displayed in yellow in Fig. 1), consistent with its attributed sensory modality, is seen to comprise the auditory cortex lying in the superior temporal gyrus of the temporal lobe (as well as, the corresponding association areas), and the medial geniculate nucleus in the thalamus, which is the relay for all auditory information destined for the cortex from the brainstem [72]. Third, module 2 (displayed in red in Fig. 1) contains the primary and secondary somatosensory areas (S1, S2) in the parietal lobe, while its thalamic component contains all the areas which together comprise the ventral posterior nucleus that relays somatosensory information to the cortex. Apart from its sensory function, as noted earlier it also consists of primary and supplementary motor areas which are associated with planning, control and execution of voluntary movements [73]. Finally, we note that module 1 (displayed in blue in Fig. 1), has the *olfactory complex* and the *gustatory cortex*, both located in the frontal lobe, as well as, a few other areas (e.g., the olfactory field of the entorhinal cortex, EO, in the temporal lobe) involved in the sensory processing of smell. However, the module is dominated by association areas located in the prefrontal cortex which are involved in high-level multimodal sensory integration and decision-making [74–78].

In contrast to the other modules, module 3 neither contains motor areas nor does it include any primary or secondary sensory areas. This is possibly related to our earlier observation that this module has a distinct structural arrangement, in that its subcortical components do not have any contribution from the thalamus, but instead comprise areas belonging to the basal ganglia. In particular, the module contains the entire *amygdala* which is known to regulate emotional responses and fear-conditioning in mammals [79–82]. This gains significance in light of the fact that both the *Hippocampus* and the *Parahippocampus*, which are primarily involved in the formation of memory, feature prominently among this

module’s cortical components. It resonates with the known relation between emotional state and formation of memories in individuals that have been established by several studies [83–86].

As the brain is characterized by structures occurring at several hierarchical levels [87], it is pertinent to ask whether a further degree of organization can be identified in the connectivity pattern within each of the modules described above. Indeed, when we consider module 5, the most robust under different realizations of network partitioning (see next subsection), and subject it to further modular decomposition, we observe that it comprises three communities which we refer to as submodules. The largest of these (5A) contains the visual cortex and almost the entirety of the subcortical components, while the other two (5B and 5C, which are comparable to each other in terms of the number of constituent areas) are dominated by areas belonging to the superior temporal sulcus and the intraparietal sulcus, respectively (Fig. 2). Intriguingly, we note that the latter two communities appear to correspond to areas identified with distinct visual processing pathways, viz., the dorsal and ventral streams [88,89]. This suggests that even at the submodular scale, network communities can be associated with specialized functions.

B. Establishing the robustness of the modular decomposition

While network communities can be defined using one of several possible approaches [90], a large number of techniques for partitioning networks are based on the principle of maximizing the metric Q [91], which quantifies the extent to which a network is modular. As mentioned in Sec. II, we have ensured that the partitioning of the connectome is not sensitively dependent on the specific method used for the decomposition. Figure 3(a) shows the communities obtained using the Infomap method [46], which is based upon optimally compressing information about dynamic processes on the network. Note that, these have a high degree of overlap with the modules shown in Fig. 1 obtained using a spectral method [41] that maximizes the modularity Q (for details, see Sec. II). While the Infomap method generates a larger number of modules (viz., 17), not only are many of these extremely small (in some cases comprising only a single node), but several of them are in fact further subdivisions of the relatively fewer modules (viz., 5) obtained using the spectral method. The relatively high degree of correspondence between the partitions generated by using techniques that employ completely different principles suggests that the modular decomposition reported here is an intrinsic property of the network and is not strongly affected by the partitioning method used.

To verify that the method used for maximizing Q does not alter our results significantly, we have performed 10^3 realizations of a stochastic simulated annealing algorithm for detecting communities [45]. As mentioned in Sec. II, by comparing between these large number of optimal partitionings of the network, we can determine the extent to which the modular groupings among the different nodes is robust. Figure 3(b) shows the Modularity Q values corresponding to these realizations, using a representation such that similar partitionings (corresponding to the circles) occur close to each other in the two-dimensional plane orthogonal to the axis representing Q .

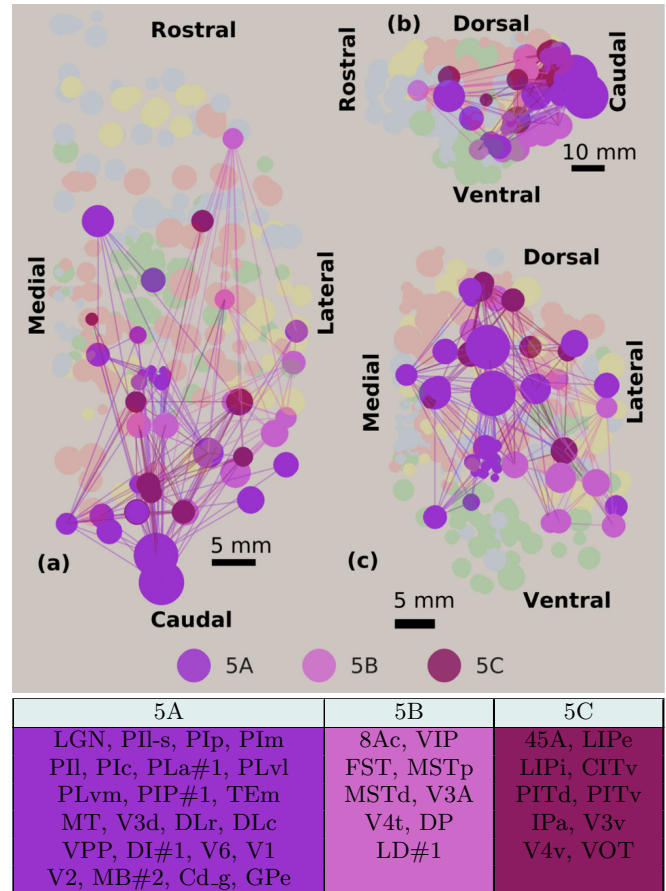


FIG. 2. Submodular organization of module 5 of the connectome. The network of brain areas, shown in (a) horizontal, (b) sagittal, and (c) coronal projections, indicate that the nodes in module 5 (highlighted), which is broadly associated with visual processing, are further organized into three submodules that are characterized by dense intraconnectivity. The submodule membership of each node in module 5 is represented by its color (see color key at the bottom) with the list of brain areas belonging to each of the three submodules shown in the table at the bottom. Submodule 5A is seen to comprise primary visual and subcortical areas, while submodules 5B and 5C contain areas that belong to the ventral and dorsal visual pathways, respectively. The node sizes provide a representation of the relative volumes of the corresponding brain areas (the spatial scale being indicated by the horizontal bar in each panel). The spatial positions of the nodes are specified by the three-dimensional stereotaxic coordinates of the corresponding areas. Links indicate the directed nerve tracts connecting pairs of brain areas, and are colored in accordance with their source nodes.

The two-dimensional coordinates of each circle in this plane is obtained by Curvilinear Component Analysis (CCA, see Ref. [92]) as described in Ref. [45]. As can be seen from Fig. 3(b), there are a large number of partitionings having high values of Q that occur close to each other in the plateau and where the partition obtained from the spectral method (diamond, $Q_{\text{spectral}} = 0.485$) that has been used for our analysis is also seen. This suggests that the modular decomposition of the nodes in these high Q partitionings are similar to that determined by the spectral method. The highlighted nodes in Figs. 3(c)–3(e) indicate those brain areas (~70% of the total)

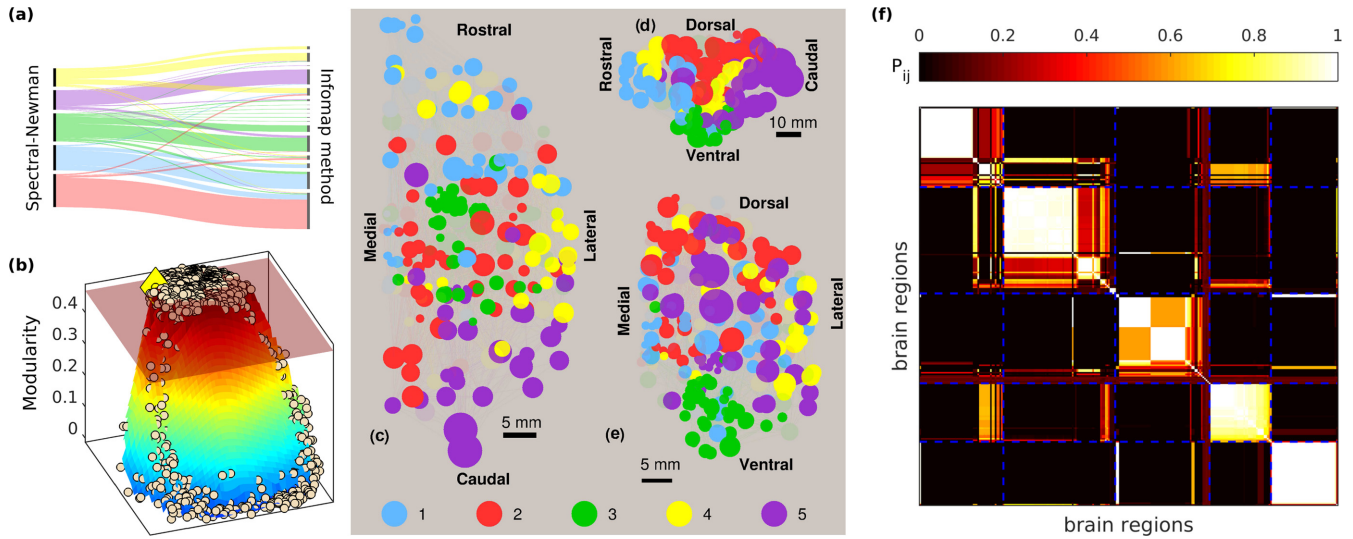


FIG. 3. Robustness of the modular decomposition of the connectome. (a) Visual representation of the comparison between the modular decomposition of the macaque connectome obtained using spectral partitioning [left] with that obtained using the Infomap method [right]. The modules are represented as vertical bars, connected by bands which are colored according to the module obtained using the spectral method from which they originate [using the same color scheme as in Fig. 1(d)]. (b) Modularity of the macaque connectome, shown as a function reconstructed from 10^3 partitionings (circles) obtained through a simulated annealing method for determining communities [45]. The axes on the horizontal plane orthogonal to the vertical axis that corresponds to modularity Q represent embedding dimensions that are themselves complex functions of the partition space, such that the scale of these axes are irrelevant. The distance between the partitionings (whose positions on the horizontal plane are obtained by Curvilinear Component Analysis) are indicative of the degree of dissimilarity between the corresponding modular partitions of the network. The partition obtained by the deterministic spectral method yielding a Q value of $Q_{\text{spectral}} = 0.485$ (diamond), and which has been used for our analysis, is seen to occur in the high-modularity plateau comprising a large number of similar partitionings, all having a high value of Q . The 291 partitionings that occur above the translucent plane corresponding to $Q = 0.47$, and whose Q values differ by less than 3% from $Q_{\text{spectral}} = 0.485$, have been used to determine the robustness of the modular identities of the different nodes in the connectome. (c–e) The network of brain areas shown in (c) horizontal, (d) sagittal, and (e) coronal projections, indicating the areas (highlighted) whose modular memberships are invariant across the partitionings obtained by the spectral method (used in our analysis) as well as those obtained by simulated annealing, whose Q differs by less than 3% from $Q_{\text{spectral}} = 0.485$. As in Figs. 1(a)–1(c), the modular membership of each node is represented by its color (see color key at the bottom of each panel), the spatial positions of the nodes are specified by the three-dimensional stereotaxic coordinates of the corresponding areas, and node sizes provide a representation of the relative volumes of the corresponding brain areas (the spatial scale being indicated by the horizontal bar shown next to each projection). Within the 291 partitionings that have $Q > 0.47$, around 70% of the 266 brain areas always occur in the same module as that in the spectral modular decomposition, underlining the robustness of their modular identities (see Supplemental Material, Table S3 [36]). This is quantitatively established by the consensus matrix shown in panel (f), which indicates for each pair i, j of brain areas the fraction of partitionings P_{ij} in which they occur in the same module. The modules obtained using spectral partitioning, displayed in the order in which they are described in the text, are indicated using broken lines. Within each module, the areas are arranged in increasing order of versatility (see text). Module 5, in particular, is seen to be almost completely consistent across all 291 partitionings.

whose modular identities remain invariant across all the partitionings whose Q differs by less than 3% from Q_{spectral} (i.e., $Q > 0.47$). In conjunction with the consensus matrix shown in Fig. 3(f) which indicates the frequency with which brain areas co-occur in the same module, this result emphasizes that the modular mesoscopic organization we have described here does not depend sensitively on the method used to partition the network. Quantifying the robustness of the modular assignment of each brain area by measuring their versatility V , i.e., the extent to which their affiliation to a module varies from one partitioning to another (see Sec. II), we observe that a large fraction ($\sim 70\%$) of them show high degree of consistency in their module membership as indicated by the corresponding low values of V (see Supplemental Material, Figs. S5 and S6 [36]). In addition, we have used multiscale techniques [29], that probes the community structure at different levels of resolution (see Sec. II), to ensure that the modules

we identify are not agglomerations of smaller modules (see Supplemental Material, Fig. S7 [36]). These observations strongly suggest that the modular organization we report here is an intrinsic property of the macaque connectome.

C. Distribution profile of nodes in terms of their intra- and intermodular connectivity is conserved across cortical and subcortical divisions

Having described the overall organizational structure of the network at the mesoscopic level, we now focus on understanding the role played by the individual brain areas in connecting other areas within their own module, as well as, across modules. The importance of each area is quantified in this framework by measuring the within-module degree z score and the intermodular participation coefficient Π^c (see Sec. II for details). As seen in Fig. 4(a), the z score allows

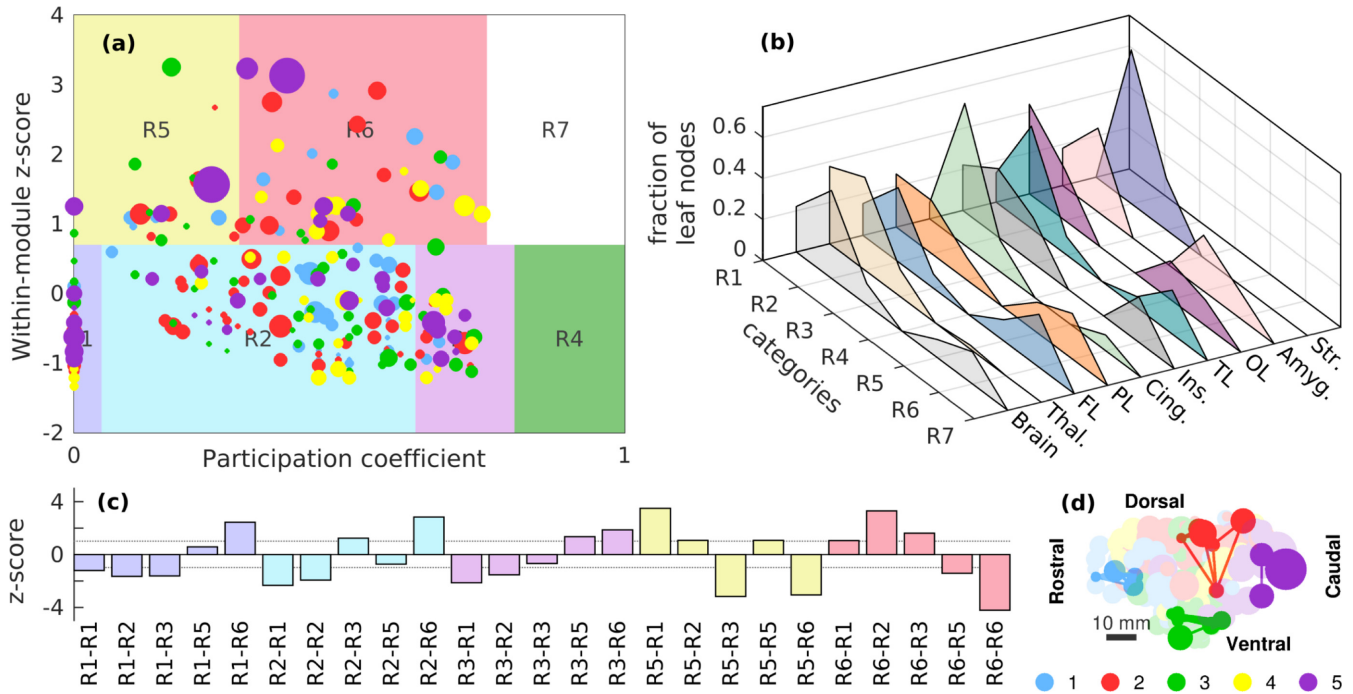


FIG. 4. Classification of brain areas according to their intra- and intermodular connectivity. (a) Nodes of the macaque brain network [colored and scaled as per Figs. 1(a)–1(c)] are displayed in accordance with their within-module degree z score (z) and participation coefficient (Π^c), which provide a measure of their intra- and intermodular connectivity respectively. This allows the brain areas to be categorized into one of seven possible categories (see Sec. II), viz., R1: ultraperipheral, R2: peripheral, R3: satellite connector, R4: kinless, R5: provincial hub, R6: connector hub, and R7: global hub. Note that there are no areas in the macaque brain belonging to the categories R4 and R7. (b) The distribution of the areas of the entire macaque brain across the different categories R1–R7 is similar to the corresponding distributions observed in several anatomical divisions, viz., *Thal*: Thalamus, *FL*: Frontal Lobe, *PL*: Parietal Lobe, *Cing*: Cingulate Gyrus, *Ins*: Insula, *TL*: Temporal Lobe, *OL*: Occipital Lobe, *Amyg*: Amygdala and *Str*: Striatum. (c) The connectivity pattern between areas belonging to the different categories R1–R7 indicated by the z scores for abundance of links between each pair of categories (the first symbol in R_i – R_j refers to the category of the source area and the second to that of the target), measured with respect to degree- and modularity-preserved randomized ensemble of networks (see Sec. II). Large positive (or negative) z scores, i.e., $z > 1$ (or $z < -1$), imply that the corresponding connection types occur more (or less) often than expected from random networks that have degree sequence and community structure identical to the empirical network (for reference, dotted lines are used to indicate $|z| = 1$). (d) Sagittal projection of the network of brain areas [see Fig. 1(b)] showing that connections between provincial hubs (highlighted nodes) are localized within each module (see Supplemental Material, Fig. S11 for an enlarged view [36]).

areas to be distinguished between *hubs*, i.e., those having significantly higher number of connections to other areas in their module, and *nonhubs*, while P further classifies the hubs into *provincial* (R5), *connector* (R6), and *global* (R7) categories and the nonhubs into *ultraperipheral* (R1), *peripheral* (R2), *satellite connector* (R3), and *kinless* (R4) classes. We note that areas in each module have a similar distribution across R1–R3 and R5–R6 (with the sole exception of module 4 which has no area playing the role of a provincial hub, see Supplemental Material, Fig. S8 [36]). Uniformity of this nature can also be observed in Fig. 4(b) where we compare the distributions of constituent areas across the different categories for the entire brain with that of the various areas of the cortex, such as the frontal (FL), parietal (PL), temporal (TL), and occipital (OL) lobes, the insula (Ins) and the cingulate gyrus (Cing), as well as a subcortical region, namely the amygdala (Amyg) which belongs to the basal ganglia. However, the striatum (Str) which is also in the basal ganglia, and the thalamus (Thal) have the distinctive characteristic of being essentially devoid of areas that act as hubs, indicating relative homogeneity in the intramodular connectivity (see Supplemental Material, Fig. S9 [36]).

We have also analyzed the relative frequency with which areas belonging to the different categories connect to each other in the macaque brain, compared to the corresponding connectivity pattern observed in surrogate networks obtained by degree- and modularity-preserving randomization (see Sec. II) [50]. The profile of connection preferences between the various categories shown in Fig. 4(c), with underrepresentation of connections between R1–R1, R5–R6, and R6–R6 which has been related to the occurrence of multistar structures, resembles other networks involved in information propagation [50]. As can also be seen from the figure, non-hubs prefer in general to connect to hubs and vice versa (see also Supplemental Material, Fig. S10 [36]). This is indicative of degree disassortativity, i.e., connections between nodes having dissimilar characteristics (in this case, the number of connections) are favored. However, on investigating the connectivity between pairs of these categories, we notice that source areas belonging to peripheral (R2) and provincial hub (R5) categories show a distinct bias in their connections in terms of the participation coefficient of the target areas. Specifically, R2 areas prefer to link to connectors, both hubs (R6) and nonhubs (R3), while avoiding areas that are localized

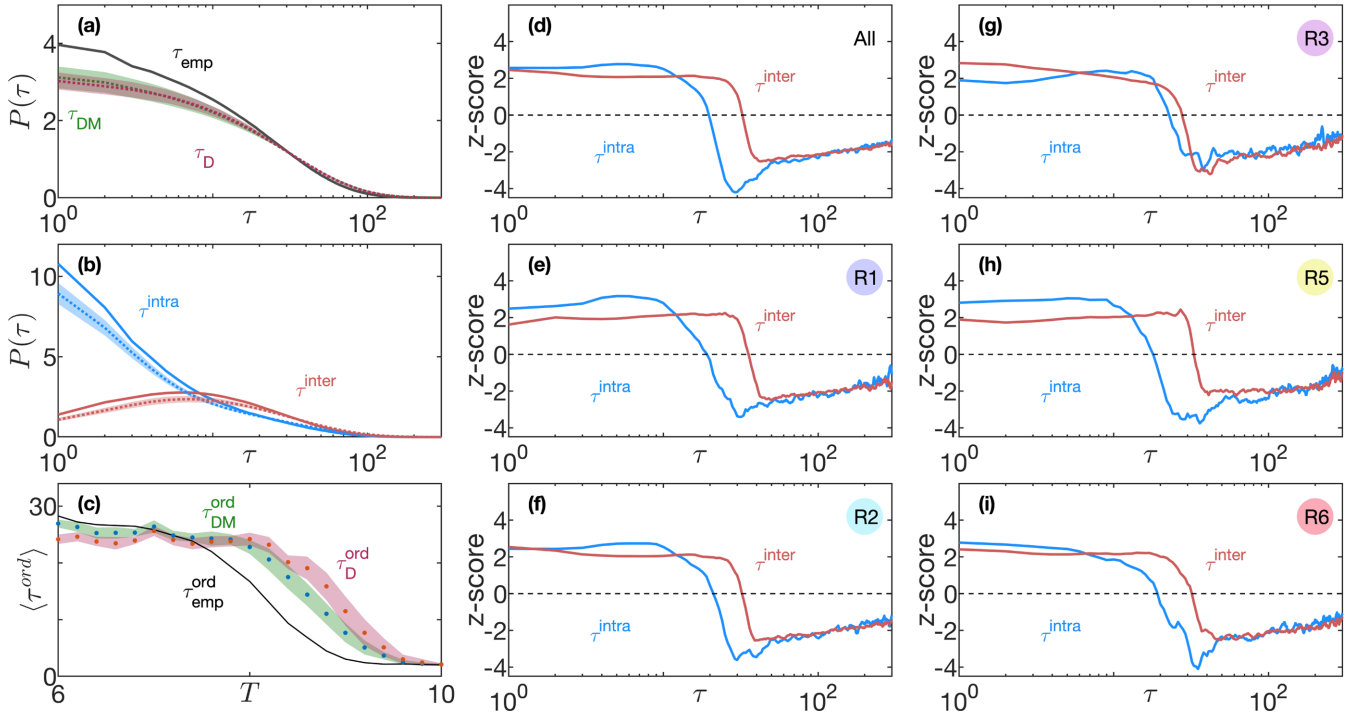


FIG. 5. The pattern of intra- and intermodular connections enhances the spread of information at local as well as global scales. (a) Temporal evolution of spreading processes, quantified in terms of distributions of first passage times (τ) of random walkers starting from one node to reach another, contrasted between the empirical brain network (solid line, τ_{emp}) and randomized ensembles of networks, generated by preserving either the degrees alone (red, τ_D), or both the degree and the modular membership of each node (green, τ_{DM}). (b) The distribution of τ differs significantly, depending on whether the target and source nodes belong to the same module (blue, τ^{intra}) or different modules (red, τ^{inter}). As in panel (a), spreading occurs significantly more rapidly in the empirical network (solid lines) compared to the networks belonging to the randomized ensemble (obtained by preserving degree and modular membership). (c) The empirical network also shows a reduction in the time (τ_{emp}^{ord}) required for global coordination, viz., the maximal ordering achieved in a system of binary Ising spins for varying fluctuation levels (indicated by the parameter T), when compared with randomized network ensembles (degree-preserved: τ_D^{ord} , degree- and module-preserved: τ_{DM}^{ord}). In panels (a)–(c), the dotted lines and the shaded regions around them represent the means and standard deviations calculated over the randomized ensembles. (d)–(i) To see how the different categories R1–R7 of brain areas allow spreading to occur faster in the empirical brain network than in equivalent randomized networks, we compare the case where the source node can belong to any category (d) with those where the source is either ultraperipheral R1 (e), peripheral R2 (f), satellite connector R3 (g), provincial hub R5 (h), or global hub R6 (i). The z score indicates that there is a statistically significant shift in the empirical distribution towards lower values of τ in all cases. However, while for R3 the increase in the rate of spreading is similar irrespective of whether the target is in the same module or in a different one, we observe that there is a relatively larger shift at lower values for τ^{intra} as compared to τ^{inter} for most of the other categories (in particular, R1 and R5). Indeed, the latter behavior dominates when we consider sources across all categories [see panel (c)].

in their modules (R1, R2, and R5). The trend is reversed for R5 areas. In particular, they show a slight preference for connecting to each other, which is in contrast to the other categories which exhibit a marked tendency to avoid others of their own kind.

This homophily between provincial hubs could arise from two different patterns of connectivity between them, viz., one in which connections between the R5 areas are confined within the same module and another in which the corresponding areas across different modules are connected. Figure 4(d) shows that the empirical evidence supports the former arrangement where, within each module, provincial hubs connect to each other preferentially. We note that the three R5 areas indicated in module 5 occur, respectively, in the three different submodules that were identified in the previous subsection. This intramodular connectivity within provincial hubs, taken together with the observation that they preferentially connect to peripheral areas while avoiding connectors,

suggest that they help coordinate activity locally within each module.

D. Information spreading within the brain is enhanced by the specific pattern of intra- and intermodular connections

The roles played by areas belonging to different categories in facilitating the transmission of information within and between modules can be investigated by considering a process of diffusive propagation across the network (see Sec. II). The distribution of first passage times τ , i.e., the time elapsed between initiating a random walk from any source node and the earliest arrival to any given target node, is shown in Fig. 5(a). While, in general, presence of modules in networks leads to slower global diffusion [25], surprisingly we observe that the distribution for the empirical network is markedly shifted towards lower values of τ compared to randomized networks with an identical degree sequence that may or may not have

modular organization. This indicates that, instead of leading to information encapsulation, the specific pattern of intra- and intermodular connections between brain areas belonging to different categories actually promotes faster communication across the network. Moreover, as seen from Fig. 5(b), the enhancement of the rate of diffusion in the connectome (in comparison to the randomized surrogates) can be seen both for transmission within a module, as well as, between different modules. To show that these results are not sensitive to the specific mechanism used to study spread of information, we perform a similar investigation using a model of collective coordination. In particular, we use the well-known Ising model wherein binary-state spins, each placed at a node of the network, attempt to align their orientations with those at neighboring nodes from which they receive connections. This tendency to order is countered by the presence of fluctuations, directly related to the “temperature” T . The extent of coordination achieved through such interactions mediated by the network is measured by an order parameter m (see Sec. II). The time required for the system to attain the steady-state value of m for a given T indicates how rapidly the influence of a node disseminates across a given network, providing an alternative means of quantifying the rate of information spreading. Figure 5(c) shows that for a range of values of T , the empirical network attains the steady state faster than the ensembles of randomized networks, reinforcing the conclusion that the specific pattern of intra- and intermodular connections occurring in the former enhances global coordination.

We also investigate how nodes belonging to each of the categories characterized by distinct intra- and intermodular connectivity roles contribute to enhancing communication in the network [Figs. 5(d)–5(i)]. This is achieved in each case by having the source node belong to the respective category and comparing the corresponding distribution of τ with that obtained from randomized surrogates (quantified using z score, see Sec. II). Figure 5(g) shows that starting from a satellite connector R3, diffusion to other nodes belonging both within its module or to other modules is significantly faster compared to randomized networks with identical modular organization and degree distribution. In contrast, as seen from Fig. 5(h), when starting from a provincial hub R5, the increase in the rate of diffusion within a module, compared to that in the surrogate networks, is even higher than the increase in the rate of diffusion across modules. This resonates with the observation of homophily between provincial hubs in a module reported earlier [Fig. 4(d)]. When the source node belongs to any of the other categories, the difference between the intra- and intermodular diffusion timescales is seen to lie between the range seen for these two cases. This suggests that the modular character of the mesoscopic organization of the connectome is further shaped by the distribution of roles played by the different nodes in allowing information to spread within a module, as well as, across different modules.

E. Spatial layout constrains the connectivity but does not determine the modular organization of the brain

So far we have investigated the modular structure of the network of brain areas exclusively in terms of the connection

topology. However, the brain is also a physical system that is embedded in three-dimensional space associated with a distance metric which restricts the possible connections between its constituent areas. Such constraints arise from resource costs related to the spatial volume and transmission time associated with the connections, and the rapid energy consumption during synaptic transmission [93–100]. Thus, given that the pattern of connections between the areas is a function of the physical distance between them, we can ask to what extent are the modules a consequence of the brain being a spatially embedded network [101,102]. Indeed there have been multiple attempts to relate the community organization of connectomes to the cost of wiring between brain areas that are located far apart [29,103]. To investigate the role of spatial constraints on the structure of the brain network, we supplement the network topological information with that of the physical locations and volumes of each of the areas (shown in Figs. 1(a)–1(c); for details see Sec. II). By comparing the distributions of the physical distances d between all possible pairs of areas (connected or not) with that of only the connected pairs [top panel of Fig. 6(a)], we can obtain the dependence of the connection probability between two areas on the distance d between them. As seen from the bottom panel of Fig. 6(a), this probability decays linearly with the reciprocal of the distance, i.e., $P(C|d) \sim 1/d$, explicitly demonstrating the constraint imposed by the spatial layout of the brain areas on their connectivity.

To see if the restriction on long-range connections implied by the above constraint is responsible for the mesoscopic organization of the network we have reported here, we investigate whether the network can be partitioned into modules even after explicitly taking into account the distance dependence of the connection probability (see Sec. II for details). Thus, if the modules are exclusively a product of the distance constraint, then the deviation of the empirically obtained connection probabilities from those of the null model will be minimal, yielding a single partition comprising the entire network (the results for different surrogate networks are discussed later). In contrast to the above scenario, we find that applying the method on the brain network yields an optimal partitioning comprising seven space-independent modules indicated by the diagonal blocks demarcated by white lines in the adjacency matrix shown in Fig. 6(b) [left surface]. The probability of connections within these modules deviate strongly from the values expected from the null model as shown by the modularity matrix [Fig. 6(b), right surface]. The distance matrix [Fig. 6(b), top surface] also appears to suggest that areas belonging to the same module are, in general, physically closer to each other than those belonging to different modules. Indeed, this is also true for the spatial clustering of nodes in each network module seen in Figs. 1(a)–1(c). However, this physical proximity cannot provide a causal explanation for the modular structure as, even after filtering for spatial effects, the resulting space-independent modules are substantially similar to those reported in the previous subsections [see Fig. 6(c)]. The similarity between the results of these two different modular partitionings is quantitatively indicated by the corresponding normalized mutual information I_{norm} ($= 0.6$) (see Sec. II). Thus, the spatial layout of the brain areas cannot by themselves explain the mesoscopic organization of

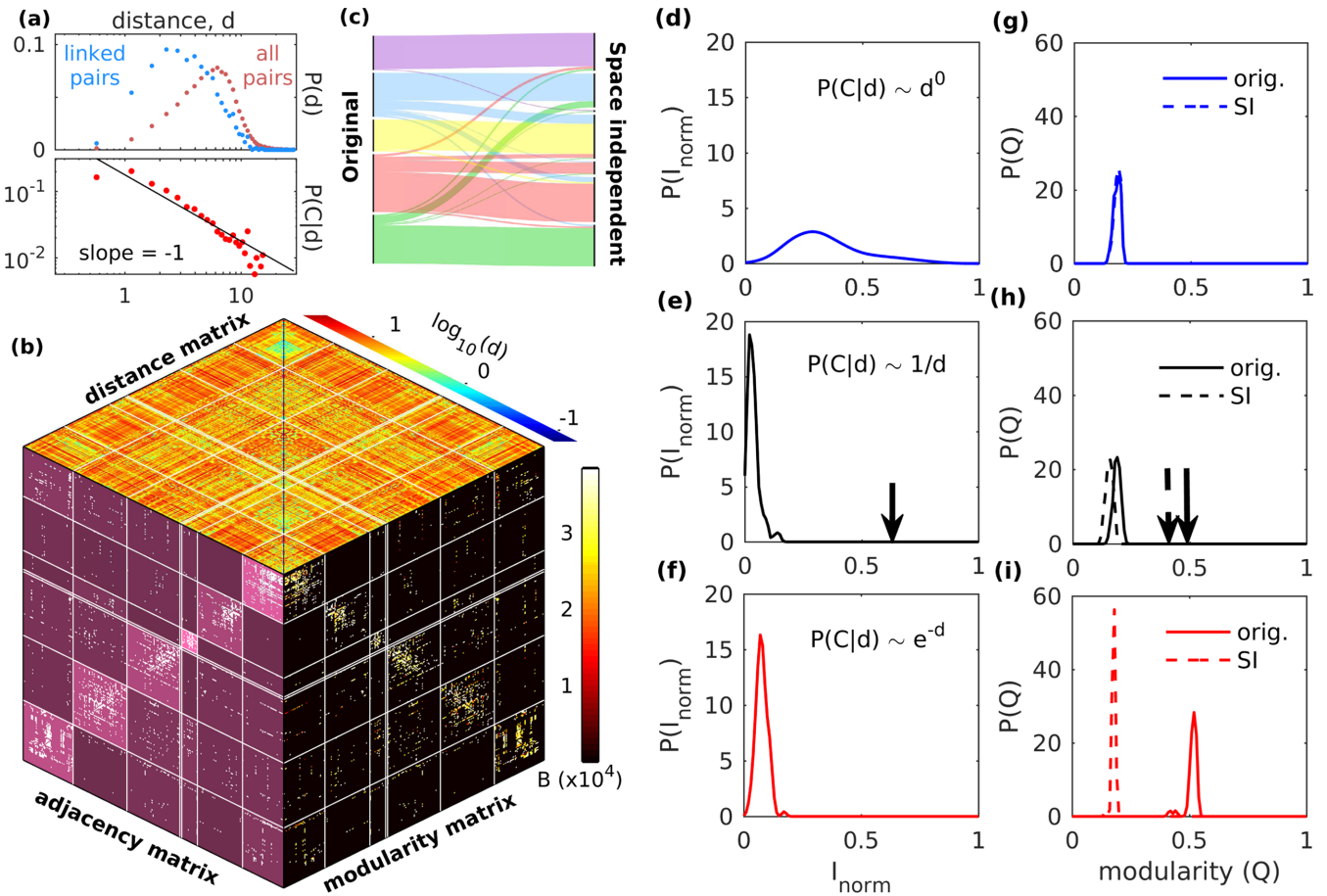


FIG. 6. Physical distance between brain areas is seen to constrain their connectivity, but the modular organization of the network is independent of their three-dimensional spatial arrangement. (a, top) Probability distribution of the physical distances d between all pairs of nodes (red) contrasted with that of connected pairs (blue). (a, bottom) The variation with physical distance d of the connection probability $P(C|d)$ between a pair of nodes separated by d (red) showing the best fit relation $P \sim 1/d$ (solid line). (b) Joint representation of the space-independent modular organization of the network of brain areas showing the matrices indicating adjacency $\{A_{ij}\}$ (left surface), modularity $\{B_{ij}\}$ (normalized by total number of links L , right surface), and physical distance $\{d_{ij}\}$ between areas. Note that for matrix **A** the background intensity of each block is proportional to the density of connections within that block, and for matrix **B** only the values corresponding to linked pairs of nodes are shown. The nodes are grouped into partitions corresponding to the space-independent modules of the network with the boundaries indicated by solid lines. The relatively large positive values clustered along the diagonal blocks of **B** indicate the occurrence of significantly higher density of connections within each module, compared to that expected from the degrees of, and the distance between, every pair of nodes. This characteristic signature of modularity is also visible in the adjacency matrix **A** representing the connection topology, suggesting that the mesoscopic structure of the brain network is a consequence of factors beyond the constraints associated with physical distance. This is also apparent from the distance matrix which shows that the modules comprise many spatially proximal nodes even after discounting the effect of distance in identifying the modules. (c) Representation of the correspondence between the network modules determined using exclusively information about the connection topology (“Original”) and those obtained from *space-independent* partitioning of the network into communities. (d)–(f) The distributions of the degree of similarity between the original topological (orig.) and the space-independent (SI) modular partitionings of a network, as measured by normalized mutual information I_{norm} for three types of random surrogate network ensembles. The corresponding values for the modularity Q obtained using the two methods is shown in panels (g)–(i). The ensembles differ in the nature of dependence of connection probability P between a pair of brain areas on the distance d between them, viz., (i) $P \sim d^0$ (d), (g), $P \sim 1/d$ (e, h), and $P \sim \exp(-d)$ (f), (i). As the macaque connectome exhibits a power-law dependence similar to that in (e) and (h), we have indicated in these panels the corresponding values for the empirical network (arrows).

the network, and the existence of the structural modules is a fundamental attribute of the brain.

To further establish that modular organization of the connectome is not primarily driven by constraints imposed by the physical distance between the brain areas, we use three classes of surrogate random network ensembles to investigate how spatial embedding affects the modular decomposition of a network, with all the nodes occupying the same

positions in physical space as in the macaque connectome. The three ensembles we have chosen for our investigation are specified by the dependence of the connection probability P between areas on the physical distance d between them, viz., (i) $P \sim d^0$, i.e., independent of the distance, (ii) $P \sim 1/d$, i.e., power-law dependence as in the empirical network, and (iii) $P \sim \exp(-d)$, i.e., exponential dependence, for which the constraint of distance most strongly

affects the probability of connection. For each category, we have generated 100 different networks that have identical numbers of nodes and links as the empirical connectome. Subsequently, we subject these networks to community detection techniques using information about the connection topology alone, as well as space-independent modular decomposition which explicitly accounts for the dependence of P on d (see above).

Figures 6(d)–6(f) shows how the modular nature of the networks belonging to each of the three ensembles mentioned above vary upon using two approaches for identifying the modules, viz., (i) using the topological information about the connections alone and (ii) employing a space-independent partitioning that takes into account the dependence of the probability of connections between areas on the physical distance between them. The similarity between the modules obtained using these two methods is measured using normalized mutual information I_{norm} (see Sec. II). Note that, if the two types of partitionings yield identical modules, then $I_{\text{norm}} = 1$, while $I_{\text{norm}} = 0$ implies maximal dissimilarity. Without any spatial dependence, the identified modules arise through fluctuations alone, and hence the similarity between the partitions obtained by the two methods will be entirely stochastic in nature, resulting in the broad distribution for I_{norm} seen in Fig. 6(d). In contrast, the ensemble underlying the distribution shown in Fig. 6(e) has an inverse relation between connection probability and physical distance, as in the empirical network. The value of I_{norm} obtained for the empirical network (indicated by the arrow) is seen to be significantly larger than those for the random ensemble. This suggests that had the modules arisen exclusively from a distance-dependent constraint on connections, the topological and space-independent approaches would have yielded highly dissimilar partitionings. Qualitatively similar results are obtained when the dependence of connection probability on physical distance is even stronger, viz., P decaying exponentially with d as in the case of the ensemble whose I_{norm} distribution is shown in Fig. 6(f). The fact that partitioning the empirical network using either the topological or the space-independent approach results in relatively similar modular decompositions suggests that constraints other than those related to physical distance plays a significant role in shaping the mesoscopic organization of the macaque connectome. The results described above are supported by the corresponding distributions of the modularity Q measured for the different partitionings obtained using each of the two approaches [broken and solid curves in Figs. 6(g)–6(i)]. Thus, in the absence of any spatial dependence, the distributions of Q obtained using the topological and the space-independent approaches completely overlap [as seen in Fig. 6(g)]. When $P \sim d^{-1}$, the relatively weak spatial dependence gives rise to marginally lower values of Q for the partitionings obtained using the space-independent method, as compared to those obtained using the topological information alone. This is seen to be true for both the empirical network (broken and solid arrows) and the random ensembles [Fig. 6(h)]. With the stronger spatial dependence inherent in an exponentially decaying functional relation, we expect to see much larger differences in the Q values for the two types of partitionings, and this is indeed observed in the distributions shown in Fig. 6(i). Therefore, the more dominant the role of

the constraint on physical distance in determining the connections, the more dissimilar the partitionings obtained by the two methods and the larger the difference in the corresponding Q values (see also Supplemental Material, Fig. S12 [36]).

IV. DISCUSSION

A. The utility of modularity in complex networks

We note that the modular nature of the brain has been long recognized, both in terms of function and, more recently, in the topological organization of its structural connections [16]. Considerable attention has been focused on the question of structure-function convergence in the context of brain modules [23]. The hypothesis of “information encapsulation,” whereby it is assumed that the information processing related to specific functions are relatively unaffected by those corresponding to other functions, has been suggested as an explanation of how functional modules can arise from the structural organization of the connectome into several communities [104]. Although this may appear intuitive because spreading processes are generally fast within a module and slow down during their passage to a different module [25], we find on the contrary that the specific modular organization of the macaque connectome allows signals to spread very fast. In fact, the communication of information across the empirical network appears to be even faster than that seen in equivalent networks whose connections are distributed homogeneously. This is surprising as global propagation is fastest for homogeneous networks, and usually tends to reduce once mesoscopic structural features such as modularity are introduced [25].

We connect this counterintuitive result to the detailed mesolevel attributes of the topological organization, specifically the roles played by different brain areas in terms of their intra- and intermodular connections. By analyzing these connections we reveal distinctive features of the connectome, namely, the tendency of provincial hubs within a module to connect to each other (R5 homophily), and the preference shown by connector hubs to link to peripheral nodes across different modules. We also note that the different regions of the brain exhibit similar distributions of intra- and intermodular connectivity roles among their constituent areas, suggesting an uniformity in the design of the network architecture across this complex system that could potentially embody a general computational logic [105,106].

The surprising role of the specific pattern of intra- and intermodular links in the macaque connectome in enabling rapid dissemination globally through the system, which we have verified using general models of diffusion, as well as, of coordination, has implications beyond the immediate context of brain networks. To illustrate this, we can compare the profile of connection preferences between nodes in the different categories R1, ..., R6 [Fig. 4(c)] with those reported for other types of networks, e.g., with networks involved in transportation and those concerned with communication [50]. In networks of the former type, links between ultraperipheral nodes (R1–R1), between connector hubs (R6–R6), and between connector and provincial hubs (R5–R6) are overrepresented, while the opposite is true for networks of the latter type. These link classes are underrepresented in the macaque connectome,

which places it among the networks concerned primarily with efficient signal transmission across the nodes, such as protein interactomes and the Internet [50]. However, the overrepresentation of connections between provincial hubs that is seen in the macaque connectome is not present in these networks. It is however a signature it has in common with another connectome, albeit at a different scale, viz., the neuronal network of *Caenorhabditis elegans* [11]. Thus, potentially it could be a characteristic feature of networks whose function involves not only conveying signals rapidly from one node to another, but to also *process* the information so that the system can mount a global response to stimuli with a high degree of reliability. Another striking feature is the preference of satellite connectors (R3) to be linked to hubs. Taken in conjunction with the R5 homophily which promotes intramodular communication, it suggests that the satellite connectors connect the provincial hubs of different modules with each other—effectively implementing an architecture that can support rapid global communication. It would be intriguing if this pattern is seen to occur in other modular networks whose principal function involves fast dissemination of information.

B. Structure-function relation in the macaque brain

Despite differences in the details of their organization, the modules that we have identified in the macaque connectome have common structural features. Most notably, each of them have cortical and thalamic components with the sole exception of module 3, suggesting a distinct functionality of this module. As mentioned in Sec. III A, each sensory modality is exclusively associated with a particular module. Thus, the sizable thalamic contribution to modules 2, 4, and 5 can be understood in terms of the roles that their cortical components play in processing specific types of sensory stimuli. In particular, the information from the corresponding sensory organs arrive at the cortical areas belonging to these modules via relay centers located in the thalamic component of the respective modules. This, however, cannot explain the sizable contribution from thalamic areas to module 1, as the sensory modalities it is associated with, namely, olfaction and gustation, do not involve any thalamic relay. As one of the primary functions of this module is the integration of information processed in different cortical areas (as mentioned earlier), it suggests that areas in the thalamic component of this module serve as relay centers coordinating intercortical communication [63].

The module with which a particular brain area is associated may also alert us to possible functions of this area that have not yet been identified. As an example we consider multimodal association areas, which integrate and process inputs from different sensory modalities (such as the areas LIP, MIP and area 46). Using information about their modular membership, we can identify which modality or function each of these areas are most strongly associated with. This is illustrated by considering the LIP, VIP, AIP and MIP areas of the *Intraparietal Sulcus*. Although they are all multimodal association areas, LIP and VIP are part of module 5, whereas areas AIP and MIP are part of module 2. It is known that LIP and VIP are involved in visual attention and saccadic eye movements [107–109], which are predominantly visual processing tasks

(consistent with the broad function of module 5). In contrast, AIP and MIP coordinate the visual control of reaching and pointing [110–112], which, although guided by visual information, is primarily a motor function (consonant with the broad function of module 2). Thus, the specific functionalities of these association areas seem to tie in with the modules that they belong to. We would also like to note that by partitioning the modules further using decomposition techniques similar to those applied on the entire connectome, one can in principle obtain submodules of brain areas that may also be functionally specialized. As described in Sec. III A, this has been done explicitly for the module 5 whose composition is the most robust under different realizations of the decomposition. The three communities thus identified can indeed be broadly associated with distinct aspects of visual processing (Fig. 2). It suggests the possibility of using information about community membership at finer scales of resolution in the mesoscopic organization to potentially identify the functional roles of specific brain areas.

We note that our work parallels the viewpoint proposed in several earlier studies that cognitive processes in the brain necessarily involve integration of information across modalities and functionalities [113–115]. For instance, behavioral studies in humans show that processes such as attention and perception could be linked to both spatial cognition and the semantic processing of language [116]. Indeed, cross-modal integration has been investigated extensively in the context of semantic comprehension [117]. The simultaneous processing of multiple inputs is believed to operate under mutual constraint satisfaction [118], with the probability estimate of each input constraining those of other inputs. Neurocomputational frameworks such as the “hub and spoke model” [119–121] have been used to suggest that modality specific sources of information (spokes) are integrated in a transmodal hub to generate conceptual knowledge. There is also substantial evidence in support of integration across different modalities occurring in primates [122–125]. Our results show that the mesoscopic organization of the modules, which individually are reminiscent of the information encapsulation perspective, can nevertheless enhance communication across the connectome, thereby promoting integration globally [115].

While the potential of rapid communication between different areas, made possible by the underlying modular architecture of the network, suggests a plausible explanation for the evolution of the observed mesoscopic organization of the macaque brain, it could also potentially be a consequence of optimizing for wiring lengths [126]. However, we have explicitly shown that the constraint imposed by the physical distance between the brain areas is insufficient to explain the modular partitions observed by us. Indeed, although the five modules of the connectome that we have identified comprise brain areas that are, for the most part, spatially proximal, module 4 is a prominent exception. It spans two widely separated locations in the brain, one comprising the primary and secondary auditory areas which are in the temporal lobe and the other consisting of association areas located in the prefrontal lobe. While it is well-established that the temporal lobe areas belonging to this module contribute to its associated sensory modality, viz., auditory processing, it is not entirely clear what role the prefrontal areas of this module plays in this context.

We note, however, that there are intriguing parallels between these areas and those occupying corresponding locations in the human brain. Specifically, the prefrontal and temporal parts of module 4 that are known to have a role in social cognition in primates [127,128] correspond to the Broca's and Wernicke's areas in the human brain, respectively. As is well known, the former is responsible for speech production in humans, while the latter is critical for language comprehension [73]. Although there is no direct counterpart of language in macaques, nonhuman primates are known to be capable of communicating through signals such as facial expressions and vocalizations [129]. This correspondence therefore warrants consideration of whether some of the areas in module 4 of the macaque brain developed from a common evolutionary precursor of the apparatus responsible for facilitating language in humans. Indeed, this view is supported by recent

research [130–132] that have used language-like behavior in nonhuman primates as models for understanding how speech and language might have evolved in humans [133].

ACKNOWLEDGMENTS

S.N.M. has been supported by the IMSc Complex Systems Project (12th Plan), and the Center of Excellence in Complex Systems and Data Science, both funded by the Department of Atomic Energy, Government of India. The simulations and computations required for this work were supported by High Performance Computing facility (Nandadevi and Satpura) of The Institute of Mathematical Sciences, which is partially funded by DST. We thank Raghavendhra Singh, Sridharan Devarajan, Dipanjan Ray, and Abhinove Nagarajan for helpful discussions.

-
- [1] K. Zilles and K. Amunts, Centenary of Brodmann's mapconception and fate, *Nat. Rev. Neurosci.* **11**, 139 (2010).
- [2] J. Jung, L. L. Cloutman, R. J. Binney, and M. A. L. Ralph, The structural connectivity of higher order association cortices reflects human functional brain networks, *Cortex* **97**, 221 (2017).
- [3] A. Goulas, R. F. Betzel, and C. C. Hilgetag, Spatiotemporal ontogeny of brain wiring, *Sci. Adv.* **5**, eaav9694 (2019).
- [4] L. W. Swanson and M. Bota, Foundational model of structural connectivity in the nervous system with a schema for wiring diagrams, connectome, and basic plan architecture, *Proc. Natl. Acad. Sci. USA* **107**, 20610 (2010).
- [5] P. T. Fox and K. J. Friston, Distributed processing; distributed functions? *Neuroimage* **61**, 407 (2012).
- [6] K. Friston, Beyond phenology: What can neuroimaging tell us about distributed circuitry? *Annu. Rev. Neurosci.* **25**, 221 (2002).
- [7] G. Deco, V. K. Jirsa, P. A. Robinson, M. Breakspear, and K. Friston, The dynamic brain: From spiking neurons to neural masses and cortical fields, *PLoS Comput. Biol.* **4**, e1000092 (2008).
- [8] J. W. Scannell, G. A. P. C. Burns, C. C. Hilgetag, M. A. O'Neil, and M. P. Young, The connective organization of the cortico-thalamic system of the cat, *Cerebral Cortex* **9**, 277 (1999).
- [9] C. C. Hilgetag, G. A. P. C. Burns, M. A. O'Neill, J. W. Scannell, and M. P. Young, Anatomical connectivity defines the organization of clusters of cortical areas in the macaque and the cat, *Philos. Trans. R. Soc. B* **355**, 91 (2000).
- [10] D. S. Bassett, D. L. Greenfield, A. Meyer-Lindenberg, D. R. Weinberger, S. W. Moore, and E. T. Bullmore, Efficient physical embedding of topologically complex information processing networks in brains and computer circuits, *PLoS Comput. Biol.* **6**, e1000748 (2010).
- [11] R. K. Pan, N. Chatterjee, and S. Sinha, Mesoscopic organization reveals the constraints governing *caenorhabditis elegans* nervous system, *PLoS One* **5**, e9240 (2010).
- [12] Q. Wang, O. Sporns, and A. Burkhalter, Network analysis of corticocortical connections reveals ventral and dorsal processing streams in mouse visual cortex, *J. Neurosci.* **32**, 4386 (2012).
- [13] L. Harriger, M. P. Van Den Heuvel, and O. Sporns, Rich club organization of macaque cerebral cortex and its role in network communication, *PLoS One* **7**, e46497 (2012).
- [14] M. Shanahan, V. P. Bingman, T. Shimizu, M. Wild, and O. Güntürkün, Large-scale network organization in the avian forebrain: A connectivity matrix and theoretical analysis, *Front. Comput. Neurosci.* **7**, 89 (2013).
- [15] C.-T. Shih, O. Sporns, S.-L. Yuan, T.-S. Su, Y.-J. Lin, C.-C. Chuang, T.-Y. Wang, C.-C. Lo, R. J. Greenspan, and A.-S. Chiang, Connectomics-based analysis of information flow in the *drosophila* brain, *Curr. Biol.* **25**, 1249 (2015).
- [16] O. Sporns and R. F. Betzel, Modular brain networks, *Annu. Rev. Psychol.* **67**, 613 (2016).
- [17] M. A. Bertolero, B. T. T. Yeo, and M. D'Esposito, The diverse club, *Nat. Commun.* **8**, 1277 (2017).
- [18] Y. Chen, Z.-K. Zhang, Y. He, and C. Zhou, A large-scale high-density weighted structural connectome of the macaque brain acquired by predicting missing links, *Cerebral Cortex* **30**, 4771 (2020).
- [19] D. Meunier, R. Lambiotte, and E. T. Bullmore, Modular and hierarchically modular organization of brain networks, *Front. Neurosci.* **4**, 200 (2010).
- [20] R. K. Pan and S. Sinha, Modular networks emerge from multiconstraint optimization, *Phys. Rev. E* **76**, 045103(R) (2007).
- [21] N. Pradhan, S. Dasgupta, and S. Sinha, Modular organization enhances the robustness of attractor network dynamics, *Europhys. Lett.* **94**, 38004 (2011).
- [22] J. A. Fodor, *The Modularity of Mind* (MIT Press, Cambridge, MA, 1983).
- [23] H.-J. Park and K. Friston, Structural and functional brain networks: From connections to cognition, *Science* **342**, 1238411 (2013).
- [24] L. W. Swanson and J. W. Lichtman, From cajal to connectome and beyond, *Annu. Rev. Neurosci.* **39**, 197 (2016).
- [25] R. K. Pan and S. Sinha, Modularity produces small-world networks with dynamical timescale separation, *Europhys. Lett.* **85**, 68006 (2009).
- [26] C. G. Antonopoulos, S. Srivastava, S. E. d. S. Pinto, and M. S. Baptista, Do brain networks evolve by maximizing their

- information flow capacity? *PLoS Comput. Biol.* **11**, e1004372 (2015).
- [27] Y. Yamaguti and I. Tsuda, Mathematical modeling for evolution of heterogeneous modules in the brain, *Neural Netw.* **62**, 3 (2015).
- [28] D. Mumford, On the computational architecture of the neocortex, *Biol. Cybern.* **65**, 135 (1991).
- [29] R. F. Betzel, J. D. Medaglia, L. Papadopoulos, G. L. Baum, R. Gur, R. Gur, D. Roalf, T. D. Satterthwaite, and D. S. Bassett, The modular organization of human anatomical brain networks: Accounting for the cost of wiring, *Netw. Neurosci.* **1**, 42 (2017).
- [30] J. Stiso and D. S. Bassett, Spatial embedding imposes constraints on neuronal network architectures, *Trends Cognit. Sci.* **22**, 1127 (2018).
- [31] D. S. Modha and R. Singh, Network architecture of the long-distance pathways in the macaque brain, *Proc. Natl. Acad. Sci. USA* **107**, 13485 (2010).
- [32] K. E. Stephan, K. Zilles, and R. Kötter, Coordinate-independent mapping of structural and functional data by objective relational transformation (ORT), *Philos. Trans. R. Soc. B* **355**, 37 (2000).
- [33] K. E. Stephan, L. Kamper, A. Bozkurt, G. A. P. C. Burns, M. P. Young, and R. Kötter, Advanced database methodology for the collation of connectivity data on the macaque brain (CoCoMac), *Phil. Trans. R. Soc. B* **356**, 1159 (2001).
- [34] R. Kötter, Online retrieval, processing, and visualization of primate connectivity data from the CoCoMac database, *Neuroinformatics* **2**, 127 (2004).
- [35] N. T. Markov, M. M. Ercsey-Ravasz, A. Ribeiro Gomes, C. Lamy, L. Magrou, J. Vezoli, P. Misery, A. Falchier, R. Quilodran, M.-A. Gariel *et al.*, A weighted and directed interareal connectivity matrix for macaque cerebral cortex, *Cerebral Cortex* **24**, 17 (2014).
- [36] See Supplemental Material at <http://link.aps.org/supplemental/10.1103/PhysRevE.106.054304> for details, as well as citations to Refs. [134–154].
- [37] A. Pathak, S. N. Menon, and S. Sinha, Uncovering the invariant structural organization of the human connectome, [arXiv:2012.15854](https://arxiv.org/abs/2012.15854).
- [38] G. Paxinos, X. F. Huang, and A. W. Toga, *The Rhesus Monkey Brain in Stereotaxic Coordinates* (Academic Press, San Diego, CA, 2000); <https://scalablebrainatlas.incf.org/macaque/PHT00>
- [39] M. E. J. Newman, Detecting community structure in networks, *Eur. Phys. J. B* **38**, 321 (2004).
- [40] M. E. J. Newman and M. Girvan, Finding and evaluating community structure in networks, *Phys. Rev. E* **69**, 026113 (2004).
- [41] M. E. J. Newman, Modularity and community structure in networks, *Proc. Natl. Acad. Sci. USA* **103**, 8577 (2006).
- [42] S. Fortunato and M. Barthelemy, Resolution limit in community detection, *Proc. Natl. Acad. Sci. USA* **104**, 36 (2007).
- [43] J. Reichardt and S. Bornholdt, Statistical mechanics of community detection, *Phys. Rev. E* **74**, 016110 (2006).
- [44] D. J. Fenn, M. A. Porter, M. McDonald, S. Williams, N. F. Johnson, and N. S. Jones, Dynamic communities in multichannel data: An application to the foreign exchange market during the 2007–2008 credit crisis, *Chaos* **19**, 033119 (2009).
- [45] B. H. Good, Y. A. de Montjoye, and A. Clauset, Performance of modularity maximization in practical contexts, *Phys. Rev. E* **81**, 046106 (2010).
- [46] M. Rosvall and C. T. Bergstrom, Maps of random walks on complex networks reveal community structure, *Proc. Natl. Acad. Sci. USA* **105**, 1118 (2008).
- [47] A. Lancichinetti and S. Fortunato, Consensus clustering in complex networks, *Sci. Rep.* **2**, 336 (2012).
- [48] M. Shinn, R. Romero-Garcia, J. Seidlitz, F. Váša, P. E. Vértes, and E. Bullmore, Versatility of nodal affiliation to communities, *Sci. Rep.* **7**, 4273 (2017).
- [49] R. Guimerà and L. A. N. Amaral, Functional cartography of complex metabolic networks, *Nature (London)* **433**, 895 (2005).
- [50] R. Guimerà, M. Sales-Pardo, and L. A. N. Amaral, Classes of complex networks defined by role-to-role connectivity profiles, *Nat. Phys.* **3**, 63 (2007).
- [51] A. Pathak, N. Chatterjee, and S. Sinha, Developmental trajectory of *Caenorhabditis elegans* nervous system governs its structural organization, *PLoS Comput. Biol.* **16**, e1007602 (2020).
- [52] F. Abdelnour, H. U. Voss, and A. Raj, Network diffusion accurately models the relationship between structural and functional brain connectivity networks, *NeuroImage* **90**, 335 (2014).
- [53] B. Mišić, R. F. Betzel, A. Nematzadeh, J. Goñi, A. Griffa, P. Hagmann, A. Flammini, Y.-Y. Ahn, and O. Sporns, Co-operative and competitive spreading dynamics on the human connectome, *Neuron* **86**, 1518 (2015).
- [54] J. Vezoli, M. Vinck, C. A. Bosman, A. M. Bastos, C. M. Lewis, H. Kennedy, and P. Fries, Brain rhythms define distinct interaction networks with differential dependence on anatomy, *Neuron* **109**, 3862 (2021).
- [55] D. J. Amit, *Modeling Brain Function: The World of Attractor Neural Networks* (Cambridge University Press, Cambridge, UK, 1989).
- [56] J. J. Hopfield, Brain, neural networks, and computation, *Rev. Mod. Phys.* **71**, S431 (1999).
- [57] J. J. Hopfield, Neural networks and physical systems with emergent collective computational abilities, *Proc. Natl. Acad. Sci. USA* **79**, 2554 (1982).
- [58] R. Cossart, D. Aronov, and R. Yuste, Attractor dynamics of network UP states in the neocortex, *Nature (London)* **423**, 283 (2003).
- [59] M. E. J. Newman and G. T. Barkema, *Monte Carlo Methods in Statistical Physics* (Oxford University Press, Oxford, UK, 1999).
- [60] P. Expert, T. S. Evans, V. D. Blondel, and R. Lambiotte, Uncovering space-independent communities in spatial networks, *Proc. Natl. Acad. Sci. USA* **108**, 7663 (2011).
- [61] D. J. C. MacKay, *Information Theory, Inference and Learning Algorithms* (Cambridge University Press, Cambridge, UK, 2003).
- [62] M. Mauri, T. Elli, G. Caviglia, G. Ubaldi, and M. Azzi, Rawgraphs: A visualisation platform to create open outputs, in *Proceedings of the 12th Biannual Conference on Italian SIGCHI Chapter, (CHIItaly'17)* (ACM, New York, NY, 2017), pp. 28:1–28:5.

- [63] J. N. MacLean, B. O. Watson, G. B. Aaron, and R. Yuste, Internal dynamics determine the cortical response to thalamic stimulation, *Neuron* **48**, 811 (2005).
- [64] L. J. Van Hemmen and T. J. Sejnowski, eds., *23 Problems in Systems Neuroscience* (Oxford University Press, New York, NY, 2006).
- [65] M. Steriade, D. A. McCormick, and T. J. Sejnowski, Thalamo-cortical oscillations in the sleeping and aroused brain, *Science* **262**, 679 (1993).
- [66] R. W. Guillery, Anatomical evidence concerning the role of the thalamus in corticocortical communication: A brief review, *J. Anat.* **187**, 583 (1995).
- [67] S. M. Sherman and R. W. Guillery, Functional organization of thalamocortical relays, *J. Neurophysiol.* **76**, 1367 (1996).
- [68] C. M. J. Braun, M. Dumont, J. Duval, I. Hamel-Hébert, and L. Godbout, Brain modules of hallucination: An analysis of multiple patients with brain lesions, *J. Psychiatry Neurosci.* **28**, 432 (2003).
- [69] S. Sternberg, Modular processes in mind and brain, *Cogn. Neuropsychol.* **28**, 156 (2011).
- [70] M. S. Gazzaniga, Brain modules and belief formation, in *Self and Consciousness* (Psychology Press, Abingdon, 2014), pp. 96–110.
- [71] L. H. Hartwell, J. J. Hopfield, S. Leibler, and A. W. Murray, From molecular to modular cell biology, *Nature (London)* **402**, C47 (1999).
- [72] D. E. Purves, G. J. Augustine, D. E. Fitzpatrick, W. C. Hall, A.-S. E. LaMantia, J. O. McNamara, and L. E. White, *Neuroscience* (Sinauer Associates, Sunderland, MA, 2001).
- [73] E. Kandel, J. Schwartz, and T. Jessell, *Principles of Neural Science*, 4th ed. (McGraw-Hill, New York, NY, 2000).
- [74] M. E. Walton, T. E. J. Behrens, M. J. Buckley, P. H. Rudebeck, and M. F. S. Rushworth, Separable learning systems in the macaque brain and the role of orbitofrontal cortex in contingent learning, *Neuron* **65**, 927 (2010).
- [75] L. K. Fellows, The role of orbitofrontal cortex in decision making: A component process account, *Ann. N.Y. Acad. Sci.* **1121**, 421 (2007).
- [76] M. E. Walton, J. T. Devlin, and M. F. S. Rushworth, Interactions between decision making and performance monitoring within prefrontal cortex, *Nat. Neurosci.* **7**, 1259 (2004).
- [77] A. Izquierdo, R. K. Suda, and E. A. Murray, Bilateral orbital prefrontal cortex lesions in rhesus monkeys disrupt choices guided by both reward value and reward contingency, *J. Neurosci.* **24**, 7540 (2004).
- [78] E. T. Rolls, The orbitofrontal cortex and reward, *Cerebral Cortex* **10**, 284 (2000).
- [79] L. Weiskrantz, Behavioral changes associated with ablation of the amygdaloid complex in monkeys, *J. Comput. Phys. Psychol.* **49**, 381 (1956).
- [80] M. Davis, The role of the amygdala in fear and anxiety, *Annu. Rev. Neurosci.* **15**, 353 (1992).
- [81] S. Killcross, T. W. Robbins, and B. J. Everitt, Different types of fear-conditioned behaviour mediated by separate nuclei within amygdala, *Nature (London)* **388**, 377 (1997).
- [82] S. Maren, Long-term potentiation in the amygdala: A mechanism for emotional learning and memory, *Trends Neurosci.* **22**, 561 (1999).
- [83] E. A. Kensinger and S. Corkin, Memory enhancement for emotional words: Are emotional words more vividly remembered than neutral words? *Mem. Cogn.* **31**, 1169 (2003).
- [84] M. P. Richardson, B. A. Strange, and R. J. Dolan, Encoding of emotional memories depends on amygdala and hippocampus and their interactions, *Nat. Neurosci.* **7**, 278 (2004).
- [85] A. K. Anderson, P. E. Wais, and J. D. E. Gabrieli, Emotion enhances remembrance of neutral events past, *Proc. Natl. Acad. Sci. USA* **103**, 1599 (2006).
- [86] A. Tambini, U. Rimmel, E. A. Phelps, and L. Davachi, Emotional brain states carry over and enhance future memory formation, *Nat. Neurosci.* **20**, 271 (2017).
- [87] P. S. Churchland and T. J. Sejnowski, Perspectives on cognitive neuroscience, *Science* **242**, 741 (1988).
- [88] M. A. Goodale and A. D. Milner, Separate visual pathways for perception and action, *Trends Neurosci.* **15**, 20 (1992).
- [89] M. A. Goodale and A. D. Milner, Two visual pathways—Where have they taken us and where will they lead in future? *Cortex* **98**, 283 (2018).
- [90] M. T. Schaub, J.-C. Delvenne, M. Rosvall, and R. Lambiotte, The many facets of community detection in complex networks, *Appl. Netw. Sci.* **2**, 4 (2017).
- [91] A. Clauset, M. E. J. Newman, and C. Moore, Finding community structure in very large networks, *Phys. Rev. E* **70**, 066111 (2004).
- [92] J. A. Lee and M. Verleysen, *Nonlinear Dimensionality Reduction* (Springer, New York, NY, 2007).
- [93] E. Bullmore and O. Sporns, The economy of brain network organization, *Nat. Rev. Neurosci.* **13**, 336 (2012).
- [94] B. B. Averbeck and M. Seo, The statistical neuroanatomy of frontal networks in the macaque, *PLoS Comput. Biol.* **4**, e1000050 (2008).
- [95] S. Herculano-Houzel, B. Mota, P. Wong, and J. H. Kaas, Connectivity-driven white matter scaling and folding in primate cerebral cortex, *Proc. Natl. Acad. Sci. USA* **107**, 19008 (2010).
- [96] D. B. Chklovskii, Exact solution for the optimal neuronal layout problem, *Neural Comput.* **16**, 2067 (2004).
- [97] M. Kaiser and C. C. Hilgetag, Modelling the development of cortical systems networks, *Neurocomputing* **58-60**, 297 (2004).
- [98] G. Buzsáki, C. Geisler, D. A. Henze, and X.-J. Wang, Interneuron diversity series: Circuit complexity and axon wiring economy of cortical interneurons, *Trends Neurosci.* **27**, 186 (2004).
- [99] M. Ercsey-Ravasz, N. T. Markov, C. Lamy, D. C. Van Essen, K. Knoblauch, Z. Toroczkai, and H. Kennedy, A predictive network model of cerebral cortical connectivity based on a distance rule, *Neuron* **80**, 184 (2013).
- [100] J. E. Niven and S. B. Laughlin, Energy limitation as a selective pressure on the evolution of sensory systems, *J. Exp. Biol.* **211**, 1792 (2008).
- [101] M. Brede, Small worlds in space: Synchronization, spatial and relational modularity, *Europhys. Lett.* **90**, 60005 (2010).
- [102] M. Barthélemy, Spatial networks, *Phys. Rep.* **499**, 1 (2011).
- [103] Y. Chen, S. Wang, C. C. Hilgetag, and C. Zhou, Trade-off between multiple constraints enables simultaneous formation of modules and hubs in neural systems, *PLoS Comput. Biol.* **9**, e1002937 (2013).
- [104] M. Colombo, Moving forward (and beyond) the modularity debate: A network perspective, *Philos. Sci.* **80**, 356 (2013).

- [105] O. D. Creutzfeldt, Generality of the functional structure of the neocortex, *Naturwissenschaften* **64**, 507 (1977).
- [106] G. Marcus, A. Marblestone, and T. Dean, The atoms of neural computation, *Science* **346**, 551 (2014).
- [107] J. W. Gnatd and R. A. Andersen, Memory related motor planning activity in posterior parietal cortex of macaque, *Exp Brain Res* **70**, 216 (1988).
- [108] J.-R. Duhamel, C. L. Colby, and M. E. Goldberg, Ventral intraparietal area of the macaque: Congruent visual and somatic response properties, *J. Neurophysiol.* **79**, 126 (1998).
- [109] B. Pesaran, J. S. Pezaris, M. Sahani, P. P. Mitra, and R. A. Andersen, Temporal structure in neuronal activity during working memory in macaque parietal cortex, *Nat. Neurosci.* **5**, 805 (2002).
- [110] H. Sakata, M. Taira, A. Murata, and S. Mine, Neural mechanisms of visual guidance of hand action in the parietal cortex of the monkey, *Cerebral Cortex* **5**, 429 (1995).
- [111] E. N. Eskandar and J. A. Assad, Dissociation of visual, motor and predictive signals in parietal cortex during visual guidance, *Nat. Neurosci.* **2**, 88 (1999).
- [112] C. Grefkes and G. R. Fink, The functional organization of the intraparietal sulcus in humans and monkeys, *J. Anat.* **207**, 3 (2005).
- [113] A. R. Luria, *Higher Cortical Functions in Man*, 2nd ed. (Springer, New York, NY, 1966).
- [114] A. R. Luria, *The Working Brain: An Introduction To Neuropsychology* (Basic Books, New York, NY, 1973).
- [115] J. L. McClelland, Integration of information: Reflections on the theme of attention and performance XVI, in *Attention and Performance XVI: Information Integration in Perception and Communication*, edited by T. Inui and J. L. McClelland (MIT Press, Cambridge, MA, 1996), p. 633.
- [116] M. K. Tanenhaus, M. J. Spivey-Knowlton, K. M. Eberhard, and J. C. Sedivy, Using eye movements to study spoken language comprehension: Evidence for visually mediated incremental interpretation, in *Attention and Performance XVI: Information Integration in Perception and Communication*, edited by T. Inui and J. L. McClelland (MIT Press, Cambridge, MA, 1996), p. 457.
- [117] J. L. McClelland, F. Hill, M. Rudolph, J. Baldrige, and H. Schütze, Placing language in an integrated understanding system: Next steps toward human-level performance in neural language models, *Proc. Natl. Acad. Sci. USA* **117**, 25966 (2020).
- [118] D. E. Rumelhart, Toward an interactive model of reading, in *Attention and Performance VI*, edited by S. Dornič (Erlbaum, Hillsdale, NJ, 1977), p. 573.
- [119] T. T. Rogers, M. A. Lambon Ralph, P. Garrard, S. Bozeat, J. L. McClelland, J. R. Hodges, and K. Patterson, Structure and deterioration of semantic memory: A neuropsychological and computational investigation, *Psychol. Rev.* **111**, 205 (2004).
- [120] K. Patterson, P. J. Nestor, and T. T. Rogers, Where do you know what you know? The representation of semantic knowledge in the human brain, *Nat. Rev. Neurosci.* **8**, 976 (2007).
- [121] M. A. Lambon Ralph, E. Jefferies, K. Patterson, and T. T. Rogers, The neural and computational bases of semantic cognition, *Nat. Rev. Neurosci.* **18**, 42 (2017).
- [122] M. T. Wallace, L. K. Wilkinson, and B. E. Stein, Representation and integration of multiple sensory inputs in primate superior colliculus, *J. Neurophysiol.* **76**, 1246 (1996).
- [123] A. Nieder, Supramodal numerosity selectivity of neurons in primate prefrontal and posterior parietal cortices, *Proc. Natl. Acad. Sci. USA* **109**, 11860 (2012).
- [124] K. Liebal, B. M. Waller, K. E. Slocombe, and A. M. Burrows, *Primate Communication: A Multimodal Approach* (Cambridge University Press, Cambridge, UK, 2014).
- [125] Y. Chen, S. Wang, C. C. Hilgetag, and C. Zhou, Features of spatial and functional segregation and integration of the primate connectome revealed by trade-off between wiring cost and efficiency, *PLoS Comput. Biol.* **13**, e1005776 (2017).
- [126] Note that other properties of cortical areas, such as similarity in terms of their neuronal densities, have been proposed to be correlated with the probability of connection between them. See, e.g., C. C. Hilgetag, M. Medalla, S. F. Beul, and H. Barbas, The primate connectome in context: Principles of connections of the cortical visual system, *Neuroimage* **134**, 685 (2016).
- [127] J. Sallet, R. B. Mars, M. P. Noonan, J. L. Andersson, J. X. O'Reilly, S. Jbabdi, P. L. Croxson, M. Jenkinson, K. L. Miller, and M. F. S. Rushworth, Social network size affects neural circuits in macaques, *Science* **334**, 697 (2011).
- [128] M. L. Platt, R. M. Seyfarth, and D. L. Cheney, Adaptations for social cognition in the primate brain, *Phil. Trans. R. Soc. B* **371**, 20150096 (2016).
- [129] D. L. Cheney and R. M. Seyfarth, Flexible usage and social function in primate vocalizations, *Proc. Natl. Acad. Sci. USA* **115**, 1974 (2018).
- [130] B. Wilson, Y. Kikuchi, L. Sun, D. Hunter, F. Dick, K. Smith, A. Thiele, T. D. Griffiths, W. D. Marslen-Wilson, and C. I. Petkov, Auditory sequence processing reveals evolutionarily conserved regions of frontal cortex in macaques and humans, *Nat. Commun.* **6**, 8901 (2015).
- [131] C. T. Snowdon, Learning from monkey “talk,” *Science* **355**, 1120 (2017).
- [132] J. P. Rauschecker, Where did language come from? Precursor mechanisms in nonhuman primates, *Curr. Opin. Behav. Sci.* **21**, 195 (2018).
- [133] O. Kolodny and S. Edelman, The evolution of the capacity for language: The ecological context and adaptive value of a process of cognitive hijacking, *Phil. Trans. R. Soc. B* **373**, 20170052 (2018).
- [134] M. S. Graziano and T. N. Aflalo, Mapping behavioral repertoire onto the cortex, *Neuron* **56**, 239 (2007).
- [135] M. Gentilucci, L. Fogassi, G. Luppino, M. Matelli, R. Camarda, and G. Rizzolatti, Functional organization of inferior area 6 in the macaque monkey, *Exp. Brain. Res.* **71**, 475 (1988).
- [136] S. T. Carmichael, M.-C. Clugnet, and J. L. Price, Central olfactory connections in the macaque monkey, *J. Comp. Neurol.* **346**, 403 (1994).
- [137] P. Apicella, T. Ljungberg, E. Scarnati, and W. Schultz, Responses to reward in monkey dorsal and ventral striatum, *Exp. Brain. Res.* **85**, 491 (1991).
- [138] C. Baleyrier and F. Mauguier, The duality of the cingulate gyrus in monkey: Neuroanatomical study and functional hypothesis, *Brain* **103**, 525 (1980).

- [139] H. C. Evrard, T. Forro, and N. K. Logothetis, Von economo neurons in the anterior insula of the macaque monkey, *Neuron* **74**, 482 (2012).
- [140] J. D. Schall, On the role of frontal eye field in guiding attention and saccades, *Vis. Res.* **44**, 1453 (2004).
- [141] T. Manzoni, F. Conti, and M. Fabri, Callosal projections from area SII to SI in monkeys: anatomical organization and comparison with association projections, *J. Comp. Neurol.* **252**, 245 (1986).
- [142] R. A. Andersen, C. Asanuma, G. Essick, and R. Siegel, Corticocortical connections of anatomically and physiologically defined subdivisions within the inferior parietal lobule, *J. Comp. Neurol.* **296**, 65 (1990).
- [143] R. Caminiti, S. Ferraina, and P. B. Johnson, The sources of visual information to the primate frontal lobe: A novel role for the superior parietal lobule, *Cerebral Cortex* **6**, 319 (1996).
- [144] E. A. Murray, T. J. Bussey, and L. M. Saksida, Visual perception and memory: A new view of medial temporal lobe function in primates and rodents, *Annu. Rev. Neurosci.* **30**, 99 (2007).
- [145] L. Malkova and M. Mishkin, One-trial memory for object-place associations after separate lesions of hippocampus and posterior parahippocampal region in the monkey, *J. Neurosci.* **23**, 1956 (2003).
- [146] N. Matsumura, H. Nishijo, R. Tamura, S. Eifuku, S. Endo, and T. Ono, Spatial- and task-dependent neuronal responses during real and virtual translocation in the monkey hippocampal formation, *J. Neurosci.* **19**, 2381 (1999).
- [147] H. S. Courellis, S. U. Nummela, M. Metke, G. W. Diehl, R. Bussell, G. Cauwenberghs, and C. T. Miller, Spatial encoding in primate hippocampus during free navigation, *PLoS Biol.* **17**, e3000546 (2019).
- [148] M. J. Jutras and E. A. Buffalo, Recognition memory signals in the macaque hippocampus, *Proc. Natl. Acad. Sci. USA* **107**, 401 (2010).
- [149] M. Petrides, Monitoring of selections of visual stimuli and the primate frontal cortex, *Proc. R. Soc. Lond. B* **246**, 293 (1991).
- [150] M. Petrides, Impairments on nonspatial self-ordered and externally ordered working memory tasks after lesions of the mid-dorsal part of the lateral frontal cortex in the monkey, *J. Neurosci.* **15**, 359 (1995).
- [151] A. Morel, P. Garraghty, and J. Kaas, Tonotopic organization, architectonic fields, and connections of auditory cortex in macaque monkeys, *J. Comp. Neurol.* **335**, 437 (1993).
- [152] L. M. Romanski and B. B. Averbach, The primate cortical auditory system and neural representation of conspecific vocalizations, *Annu. Rev. Neurosci.* **32**, 315 (2009).
- [153] N. E. Barraclough, D. Xiao, C. I. Baker, M. W. Oram, and D. I. Perrett, Integration of visual and auditory information by superior temporal sulcus neurons responsive to the sight of actions, *J. Cogn. Neurosci.* **17**, 377 (2005).
- [154] N. J. Smelser and P. B. Baltes, eds., *International Encyclopedia of the Social & Behavioral sciences* (Elsevier, Amsterdam, 2001), Vol. 11.